Self-consistent model of magnetospheric ring current and electromagnetic ion cyclotron waves: The 2–7 May 1998 storm

G. V. Khazanov
NASA Marshall Space Flight Center, Huntsville, Alabama, USA

K. V. Gamayunov
Geophysical Institute, University of Alaska Fairbanks, Fairbanks, Alaska, USA

V. K. Jordanova
Space Science Center, University of New Hampshire, Durham, New Hampshire, USA

Received 23 January 2003; revised 8 August 2003; accepted 20 August 2003; published 3 December 2003.

[1] A complete description of a self-consistent model of magnetospheric ring current interacting with electromagnetic ion cyclotron waves is presented. The model is based on the system of two kinetic equations; one equation describes the ring current ion dynamics, and another equation describes the wave evolution. The effects on ring current ions interacting with electromagnetic ion cyclotron waves and back on waves are considered self-consistently by solving both equations on a global magnetospheric scale under nonsteady state conditions. The developed model is employed to simulate the entire 2–7 May 1998 storm period. First, the trapped number fluxes of the ring current protons are calculated and presented along with comparison with the data measured by the three-dimensional hot plasma instrument Polar/HYDRA. Incorporating in the model the wave-particle interaction leads to much better agreement between the experimental data and the model results. Second, examining of the wave (MLT, L shell) distributions produced by the model during the storm progress reveals an essential intensification of the wave emission about 2 days after the main phase of the storm. This result is well consistent with the earlier ground-based observations. Finally, the theoretical shapes and the occurrence rates of the wave power spectral densities are studied. It is found that about 2 days after the storm's main phase on 4 May, mainly non-Gaussian shapes of power spectral densities are produced. *INDEX TERMS:* 2736 Magnetospheric Physics: Magnetosphere/ionosphere interactions; 2753 Magnetospheric Physics: Numerical modeling; 2778 Magnetospheric Physics: Ring current; 2431 Ionosphere: Ionosphere/magnetosphere interactions (2736); 2483 Ionosphere: Wave/particle interactions; *KEYWORDS:* ring current, wave-particle interaction, numerical modeling, magnetosphere-inner

Citation: Khazanov, G. V., K. V. Gamayunov, and V. K. Jordanova, Self-consistent model of magnetospheric ring current and electromagnetic ion cyclotron waves: The 2–7 May 1998 storm, *J. Geophys. Res.*, *108*(A12), 1419, doi:10.1029/2003JA009856, 2003.

1. Introduction

[2] The geomagnetic storm occurs when merging of the interplanetary magnetic field with the Earth's magnetic field causes a deep and intense circulation of the magnetospheric plasma building up an energy content of the terrestrial ring current (RC) to an unusually high level [e.g., *Tsurutani and Gonzalez*, 1997]. The presence of the strong RC is one of the major features of the magnetic storms [*Gonzalez et al.*, 1994], and RC intensity is closely related to the space weather resulting from storm. The ions of magnetospheric RC have energies between energies of the thermal plasma and the particles of radiation belts, and mainly there are trapped ions with energies 10–200 keV [e.g., *Smith and Hoffman*, 1973; *Williams*, 1980, 1981]. First observations in the sixties of the last century have revealed that RC ions occupy almost the entire magnetosphere from L $\sim$ 2 up to the boundary of the closed geomagnetic field L $\sim$ 10, and the peak of the RC energy density takes place in the near-equatorial region at L $\sim$ 3.5.

[3] Energetic particles in the Earth's magnetosphere frequently have anisotropic phase space distribution functions. There is no exception for the RC ions; as a rule, the effective temperatures transverse to, $T_\perp$, and along, $T_\parallel$, geomagnetic field comply with an inequality $T_\perp > T_\parallel$. If an ion temperature anisotropy, $A = T_\perp/T_\parallel - 1$, exceeds some positive threshold, there is a possibility of generating electromagnetic ion cyclotron (EMIC) waves [*Cornwall*, 1964; *Cornwall*, 1965; *Kennel and Petschek*, 1966]. Measurements taken on boards GEOS 1 and 2 satellites have displayed a critical role of the thermal He^+ admixture for generating the EMIC waves [*Young et al.*, 1981; *Roux et al.*,

Copyright 2003 by the American Geophysical Union.
0148-0227/03/2003JA009856$09.00

1982]. These observations have stimulated an appearance of theoretical papers in which the influence of the thermal He^+ admixture on the EMIC wave generation has been studied [*Mauk*, 1982; *Roux et al.*, 1982; *Gomberoff and Neira*, 1983; *Gendrin et al.*, 1984; *Denton et al.*, 1992]. The effects of energetic RC heavy ions (He^+ and O^+) on generation of EMIC waves in a multi-ion core plasma (H^+, He^+, O^+) have also been studied by *Kozyra et al.* [1984]. One example of the wave generation driven by the temperature anisotropy is EMIC waves in the Earth's RC region [e.g., *LaBelle et al.*, 1988; *Anderson et al.*, 1992a, 1992b; *Erlandson and Ukhorskiy*, 2001]. The effects of EMIC waves on dynamics of the (1) RC ions, (2) thermal plasmaspheric electrons, and (3) thermal plasmaspheric ions are well-known examples of the wave-particle interactions in the Earth's magnetosphere. RC-EMIC wave interaction mainly causes scattering of the ions into the loss cone and leads to decay of the RC [e.g., *Cornwall et al.*, 1970], especially during the main phases of storms when the RC decay times of about 1 hour or less are possible [*Gonzalez et al.*, 1989]. The obliquely propagating EMIC waves are damping due to Landau resonance with the thermal plasmaspheric electrons, and subsequent transport of the dissipating wave energy into the ionosphere causes ionosphere temperature enhancement. This process has been employed by *Cornwall et al.* [1971] as a major physical mechanism which is able to drive SAR arc emissions during the recovery phase of the storm. Measurements taken aboard the Prognoz satellites have revealed near plasmapause a so-called hot zone where the temperature of the core plasma ions can reach tens of thousands of degrees [*Bezrukikh and Gringauz*, 1976; *Gringauz*, 1983, 1985]. In order to explain such temperature enhancement, the mechanism of nonlinear interaction of the thermal plasmaspheric ions and EMIC waves has been employed by *Gorbachev et al.* [1992].

[4] From the above brief references, it follows that the EMIC waves generated by the RC ions are widely investigated both theoretically and experimentally, and these waves are strongly driving particle dynamics in the Earth's magnetosphere.

[5] Recently, *Jordanova et al.* [1997, 1998b, 2001] developed a kinetic model of the terrestrial RC, and for the first time included a quasilinear RC-EMIC wave interaction on a global scale. An effect of wave-particle interaction on the RC distributions was included in the model by using the diffusion coefficients which were obtained for the case of a multi-ion plasmaspheric thermal plasma [*Jordanova et al.*, 1996b]. In that model the hot plasma dispersion relation of EMIC waves was employed [*Kozyra et al.*, 1984] and solved self-consistently with the RC bounce-averaged kinetic equations. Number densities, parallel and perpendicular temperatures, and temperature anisotropies of the RC H^+, O^+, and He^+ ions were obtained by taking the moments of the phase space distribution functions, and were then used to calculate the wave growth rates of EMIC waves in the bi-Maxwellian plasmas. In order to obtain the gain of EMIC waves, G, the local growth rates were then integrated along wave paths, which are field-aligned. *Jordanova et al.* [2001], using the fit $B_w = B_{sat}\, 10^{(G-G_{max})/G_{min}}$, related a calculated wave gain with the measured EMIC wave amplitudes on a basis of statistical study. The saturation value B_{sat} = 10 nT was obtained from the observations [*Anderson et al.*, 1992a, 1992b; *Bräysy et al.*, 1998], and G_{min}, G_{max} are 20 and 60 dB, respectively, i.e., the range 0.1–10 nT for B_w was adopted. On the evidence of the above semiempirical model *Jordanova et al.* [2001] obtained the global image of the growth of the He^+ EMIC wave mode and the RC proton precipitation as the 14–16 May 1997 storm evolved. It was demonstrated that unstable regions of EMIC waves are highly dynamic, located at larger L shells during prestorm conditions, moving to lower L shells during the storm's main phase, and receding back toward larger L shells with storm recovery. The most intense precipitating proton fluxes were obtained along the duskside plasmapause during the main and early recovery phases of the 14–16 May 1997 storm.

[6] It is well-known that the effects of EMIC waves on RC ion dynamics strongly depend on such particle/wave characteristics as the ion phase space distribution function, frequency, wave normal angle, wave polarization, wave energy, and form of the wave power spectral density (PSD). All these characteristics cannot be independent and should be self-consistently determined by evolution of the wave-ion system itself. In order to properly quantify the EMIC wave effects on the RC ion dynamics, a newly developed self-consistent theoretical model of ions and waves has been employed by *Khazanov et al.* [2002], who have presented some initial results and have briefly outlined the model, but descriptions and discussions of many model related details have been omitted. In the present paper, this new model is described in detail for the first time. In addition to detailed description of the model itself, we use this model to simulate the 2–7 May 1998 storm. In comparison with the case considered by *Khazanov et al.* [2002], we study here the entire storm period, focus on different characteristics of the RC-wave system, and mainly pay attention to comparisons of the model obtained wave and ion results with experimentally obtained data. First, the simulated number fluxes of trapped RC protons are presented along with the comparisons with data measured by the three-dimensional (3-D) hot plasma instrument Polar/HYDRA [*Scudder et al.*, 1995]. Second, an enhancement of Pc 1 emissions a few days after the main phases of geomagnetic storms has been observed by *Wentworth* [1964], and to theoretically examine this phenomenon, the (MLT, L shell) wave distributions are produced and investigated during the storm progress. Finally, a quasilinear interaction of EMIC waves and RC ions strongly depends on the wave/particle characteristics, particularly on the wave PSD, which itself is determined by a self-consistent evolution of the RC-EMIC wave system. In most previous studies of quasilinear wave-particle interactions, a Gaussian approximation to the shape of PSD is assumed [e.g., *Lyons*, 1974; *Abel and Thorne*, 1998a, 1998b; *Albert*, 1999; *Jordanova et al.*, 2001]. To test this assumption quantitatively, we examine the theoretical shapes and occurrence rates for PSDs of EMIC waves self-consistently generated during the studied storm.

2. Model Description

2.1. Governing Equations

[7] We simulate the RC dynamics by solving the bounce-averaged kinetic equation for the phase space distribution

function, $F(r, \varphi, E, \mu_0, t)$, of the RC species. Distribution function depends on radial distance in the magnetic equatorial plane, r (zero at the Earth's center), geomagnetic east longitude, φ (zero at midnight), kinetic energy, E, cosine of the equatorial pitch angle, μ_0, and time, t, [*Jordanova et al.*, 1996a, 1997]. EMIC waves propagate along the geomagnetic field lines and reflect at ionosphere altitudes, bouncing between conjugate ionospheres. Averaging the wave kinetic equation over the periods of "fast" wave bounce oscillations, we can obtain the equation for describing "slow" evolution of the wave PSD [*Bespalov and Trakhtengerts*, 1986]. The resulting system of two quasi-linear kinetic equations has the form [*Khazanov et al.*, 2002]:

$$\frac{\partial F}{\partial t} + \frac{1}{r^2}\frac{\partial}{\partial r}\left(r^2\left\langle\frac{dr}{dt}\right\rangle F\right) + \frac{\partial}{\partial \varphi}\left(\left\langle\frac{d\varphi}{dt}\right\rangle F\right) + \frac{1}{\sqrt{E}}\frac{\partial}{\partial E}\left(\sqrt{E}\left\langle\frac{dE}{dt}\right\rangle F\right) + \frac{1}{\mu_0 h(\mu_0)}\frac{\partial}{\partial \mu_0}\left(\mu_0 h(\mu_0)\left\langle\frac{d\mu_0}{dt}\right\rangle F\right) = \left\langle\left(\frac{\delta F}{\delta t}\right)_{loss}\right\rangle, \quad (1)$$

$$\frac{\partial\langle B^2_{\omega,\theta}\rangle}{\partial t} = \left(\ln \mathrm{R} + 2\oint \frac{\gamma}{v_g}\mathrm{d}s\right)\frac{\langle B^2_{\omega,\theta}\rangle}{T_s}, \quad (2)$$

where ds is an element along geomagnetic field line. In the left-hand side of the equation (1) all the bounce-averaged drift velocities are denoted as $\langle\ldots\rangle$ and may be found in the work of *Jordanova et al.* [1994]. The term in the right-hand side of equation (1) includes losses from charge exchange, Coulomb collisions, ion-wave scattering, and precipitation at low altitudes [*Jordanova et al.*, 1996a, 1997]. Loss through the dayside magnetopause is taken into account, allowing a free outflow of the RC ions from the simulation domain. The ion-wave collisional term, included in the right-hand side of equation (1), is a function of EMIC wave PSD which is described by the wave kinetic equation (2). In the last equation, $\langle B_{\omega,\theta}{}^2\rangle = \langle B^2(\omega, \theta, \varphi, r)\rangle$ is the squared EMIC wave spectral magnetic field averaged over the wave bounce oscillation, ω is a wave frequency, and θ is an angle between the external magnetic field line and the wave vector. Parameter R is an effective reflection coefficient from the ionosphere characterizing wave energy loss due to nonperfect reflection. The local wave growth rate in equation (2), $\gamma(\omega, \theta, \varphi, r, s)$, depends on the phase space distribution function of the RC species, and is integrated over bounce oscillation of the wave envelope. The factor $T_s/2$ is the time of group propagation of the wave signal between conjugate ionospheres, and v_g is a wave group velocity. (For more details regarding equation (2) see *Khazanov et al.* [2002]. Also, for completeness, we provide in Appendix A all the expressions for drift velocities, loss terms, growth/damping rates, and reflection index.)

2.2. Resonant Ion-Wave Interaction

2.2.1. Algorithm for Finding the Resonant Numbers

[8] The ion-wave interaction in a quasi-linear approximation is a resonant process. In homogeneous magnetoactive plasma the resonant condition is well known and has the form of equation

$$f \equiv \omega - k_\parallel v_\parallel - n\Omega = 0, \qquad n = 0,\ \pm1,\ \pm2,\ \ldots, \quad (3)$$

where $k_\parallel$, $v_\parallel$ are the components of the wave normal vector and the RC ion velocity along the geomagnetic field, and Ω is a gyrofrequency of the RC ions. (The condition in equation (3) appears in the integral expressions for diffusion coefficient and growth rate in the form of δ-function as $\delta(\omega - k_\parallel v_\parallel - n\Omega)$.) If a simulation grid is set up, it is obvious that on this grid we can practically never meet the condition in equation (3). So, some nondiscrete algorithm should be incorporated in the numerical model. We describe below the suggested algorithm considering the case of growth rate calculation, and the calculation of an ion diffusion coefficient is analogous.

[9] Discrete analog for the local growth rate may be presented as

$$\gamma = \sum_{i,j}\sum_n G_{i+1/2,j+1/2}\delta(f)\left(\overline{\Delta\mu}\right)_i\left(\overline{\Delta v}\right)_j, \quad (4)$$

where $\left(\overline{\Delta\mu}\right)_i$ and $\left(\overline{\Delta v}\right)_j$ are the sizes of (i, j)-cell in cosine of the local pitch angle and the RC ion velocity space, and function G depends on both wave and RC characteristics. We can expand the left-hand side of the resonant condition in equation (3) in a linear series with respect to the center of (i, j)-cell. The wave characteristics in equation (4) are constants. If we assume the resonant number(s) may be real number(s), then we can obtain an inequality to which the "real resonant number(s)" should meet inside the current cell

$$\frac{\omega - k_\parallel\left(v_\parallel\right)_{i+1/2,j+1/2} - 0.5\varepsilon}{\Omega} \le n \le \frac{\omega - k_\parallel\left(v_\parallel\right)_{i+1/2,j+1/2} + 0.5\varepsilon}{\Omega}, \quad (5)$$

where

$$\varepsilon = \left|\frac{\partial f}{\partial \mu}\right|_{i+1/2,j+1/2}\left(\overline{\Delta\mu}\right)_i + \left|\frac{\partial f}{\partial v}\right|_{i+1/2,j+1/2}\left(\overline{\Delta v}\right)_j.$$

If at least one integer number, n, is found between the left- and the right-hand sides of the inequality in equation (5), then the current (i, j)-cell is the "resonant cell," the found integer number(s) is(are) resonant number(s), and we can do a summation over the obtained n in order to get the contribution to growth rate from (i, j)-cell. Otherwise, if there is no integer number, n, among the solutions of the inequality in equation (5), we consider the next cell.

[10] Further, the differential form of the resonant condition has the form of equation

$$\mathrm{d}f \approx \Delta f = \frac{\partial f}{\partial \mu}(\Delta\mu) + \frac{\partial f}{\partial v}(\Delta v) = 0$$

and provides us with the relation between $(\Delta\mu)$ and (Δv) along a resonant curve. So, if (i, j)-cell is the "resonant cell" and $(\Delta\mu) \equiv \left(\overline{\Delta\mu}\right)_i$, the contribution to equation (4) from (i, j)-cell should be corrected by the factor

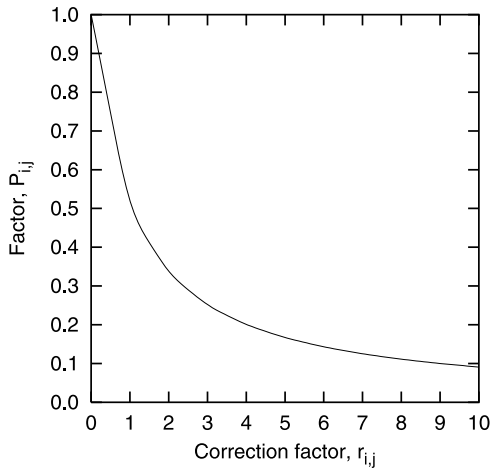

Figure 1. An additional factor $P_{i,j}$ to the right-hand side of equation (6) as a function of $r_{i,j}$.

$$r_{i,j} = \frac{\overline{(\Delta\mu)}_i}{\overline{(\Delta v)}_j} \left| \frac{\partial f}{\partial \mu} \Big/ \frac{\partial f}{\partial v} \right|_{i+1/2, j+1/2}. \tag{6}$$

The factor in equation (6) is a ratio of $|\Delta v|$, which corresponds to $\overline{(\Delta\mu)}_i$ along a resonant curve, to the v-size of (i, j)-cell. We know that the "resonant cell" contains some part of a resonant curve, but it is not necessary that the curve connects the diagonally opposite corners of (i, j)-cell. So, we do not know the actual curve position inside the cell. Meanwhile, the resonant curve position and result in equation (4) should not depend on the selected (i, j)-grid. These facts allow us to employ a statistical approach in order to take into account the curve position inside the cell. For example, if $r_{i,j} \leq 1$, then with the probability $(1 - r_{i,j})$ the part of a resonant curve corresponding to $\overline{(\Delta\mu)}_i$ will be entirely found in (i, j)-cell, and with probability $r_{i,j}$ will be found in two cells (i, j) and $(i, j + 1)$ (or $(i, j - 1)$). So, in this case an averaged correction to (i, j)-cell from the found resonant curve is $r_{i,j}(1 - r_{i,j}) + 0.5 r_{i,j} r_{i,j} = r_{i,j}(1 - 0.5 r_{i,j})$. In other words, we so introduce an additional factor $P_{i,j}$ to the right-hand side of equation (6) that the product $r_{i,j} \times P_{i,j}$ gives an averaged correction to (i, j)-cell from the found resonant curve. Factor $P_{i,j}$ depends on a magnitude of $r_{i,j}$. There is a slightly complicated expression for $r_{i,j} > 1$, and for the $r_{i,j}$ range this factor is shown in Figure 1. If on the selected grid the correction factor $r_{i,j} \approx 1$, then $P_{i,j}$ is about 0.5, and for $r_{i,j} \gg 1$ the product $r_{i,j} \times P_{i,j}$ approaches to 1.

2.2.2. Growth Rates and Diffusion Coefficients

[11] The above algorithm allows us to easily find the "resonant cell," resonant numbers, and to get the correct contribution to equation (4) from each "resonant cell." Employing this algorithm, we calculate the EMIC wave growth rates due to anisotropic RC protons and diffusion coefficients in two different core plasmas. The growth rates are presented in Figure 2. For reference we also provide the EMIC wave refractive indices in the appropriate cold plasmas. Each EMIC wave mode is shown by a distinctive color, and letters L and R mark the left-hand and the right-hand polarized branches of the waves, respectively. Results in Figure 2a are obtained for a core plasma of electrons, 77% of H^+, 20% of He^+, and 3% of O^+, which is in the range of 10–30% for He^+ and 1–5% for O^+, following observations by *Young et al.* [1977] and *Horwitz et al.* [1981] (see also the theoretical paper by *Kozyra et al.* [1984]). Pure electron-proton plasma is considered for obtaining the results in Figure 2b. In both cases the RC is entirely made up of energetic H^+. In order to calculate the EMIC wave growth rates, we used an initial phase space distribution function of the RC protons, and this function is shown in Figure 3. In a multi-ion core plasma, all the EMIC wave modes are named in accordance with the gyrofre-

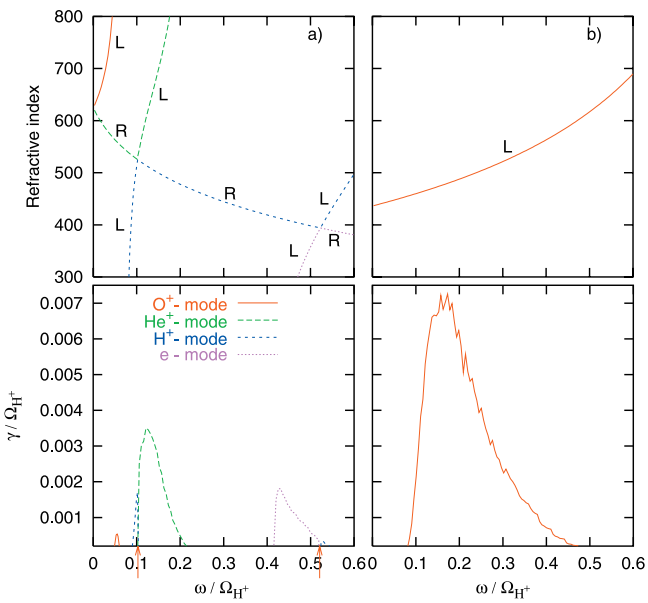

Figure 2. Equatorial refractive indices and growth rates for the quasi-field-aligned ($\theta = 2.25°$) EMIC waves at 0000 UT on 1 May 1998. L = 4.25, MLT = 17, plasmaspheric electron density is 165 cm^{-3}, the Earth's magnetic field is 405 nT, and RC ions are energetic protons. Each wave mode is shown by the distinctive color. Letters L and R mark the left-hand and the right-hand polarized branches of the waves, respectively. (a) Thermal ion composition is 77% of H^+, 20% of He^+, and 3% of O^+. Two red arrows at the figure bottom label the frequencies of polarization changing along the dispersive curves; (b) thermal plasma is entirely of electron-proton.

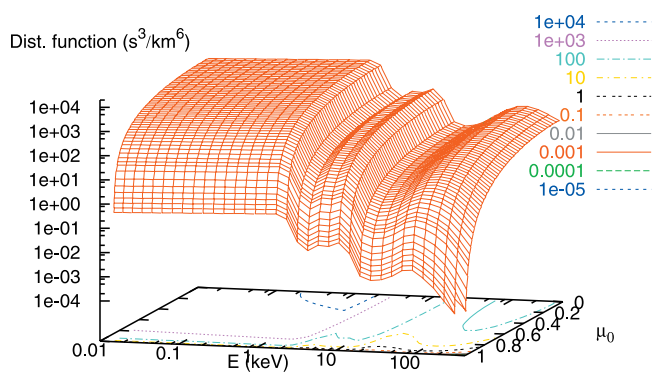

Figure 3. Equatorial RC proton distribution function at 0000 UT on 1 May 1998, L = 4.25, MLT = 17.

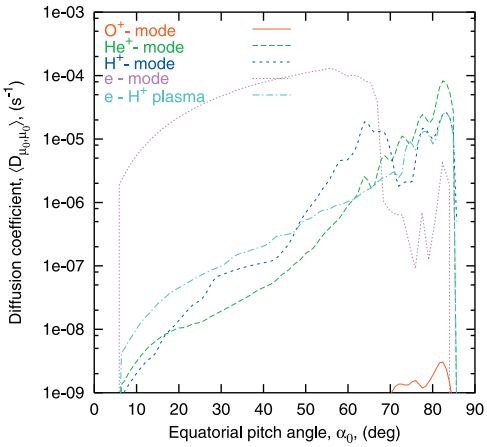

Figure 4. Bounce-averaged pitch angle diffusion coefficients for 10.8 keV RC protons interacting with EMIC waves at 0000 UT on 1 May 1998. L = 4.25, MLT = 17, boundary of the loss cone pitch angles is 5.1°, power spectral density is "white noise" and expressed as $\langle B_{\omega,\theta}{}^2\rangle$ = 1 nT^2/(rad^{2}Hz).

quencies to which the field-aligned modes approach for infinite wave numbers, i.e., there are Ω_{O^+}, Ω_{He^+}, Ω_{H^+}, $|\Omega_e|$ for O^+, He^+, H^+, and e modes, respectively. The refractive indices in Figure 2 are presented for oblique wave propagation. In this case the dispersive curves in a multi-ion thermal plasma do not cross over and do not even touch each other (see Figure 2a where $\theta = 2.25°$), but along the dispersive curves the wave polarizations are changing crossing so-called crossover frequencies (labeled by the red arrows at the bottom of Figure 2a). The situation is changing for a field-aligned wave propagation; with decreasing the wave normal angle, θ, the dispersive curves firstly touch each other and then, with further wave normal angle decreasing, cross over (at crossover frequencies) with dramatic reconstruction of the dispersive curves. Note that in the cold plasma approximation the dispersive curves cross over only for the wave normal angles $\theta = 0$ and $\theta = \pi$. In the case of a field-aligned wave propagation, the wave polarizations are conserved along each of the dispersive curves, and we get the well-known left-hand polarized bands of the EMIC wave (O^+, He^+, and H^+ bands) and fast magnetosonic wave with the right-hand polarization (it is easy to see these bands in Figure 2a if do not pay attention to the line colors). In a multi-ion thermal plasma the peak of the growth rate takes place for He^+-mode inside the frequency region in which the EMIC waves are left-hand polarized. Growth rate peak for the e-mode is about two times less than for the He^+-mode and again takes place in a region of the "left-hand polarization" of the dispersive curve. Growth rates of O^+ and H^+ modes are negligible in comparison with the other two modes. Growth rate profile in the e-p thermal plasma is wider and the peak is two times higher than for the He^+-mode (compare Figures 2b and 2a).

[12] Figure 4 demonstrates the bounce-averaged pitch angle diffusion coefficients characterizing 10.8 keV RC proton scattering rates on the EMIC waves of different modes (actually $\langle D_{\mu 0,\mu 0}\rangle$ describes diffusion in space of cosine of the equatorial pitch angle). In order to avoid an influence of PSD structure on diffusion coefficients, the PSD is set up to the "white noise," i.e., for each wave mode $\langle B_{\omega,\theta}{}^2\rangle$ is a constant inside an available (ω, θ)-region (for e-mode only frequency range $\Omega_{He^+} - \Omega_{H^+}$ is considered, and there are $\Omega_{O^+} - \Omega_{H^+}$, $0 - \Omega_{He^+}$, $0 - \Omega_{O^+}$ frequency ranges for H^+, He^+, and O^+ modes, respectively). It follows from Figure 4 that diffusion of RC ions with the equatorial pitch angles less than about 60 degrees is much faster due to interaction with the e-mode than with other modes, and the combined consideration of Figures 2a and 4 leads to the following conclusion. While the EMIC waves grow slower in the e-mode than in the He^+-mode, and as consequence less intense waves may be observed in the e-mode than in the He^+-mode, the resulting diffusion coefficient may stay bigger for e-mode than for He^+-mode. Note that we also calculated the diffusion coefficient (not shown) for the case of the e-mode considering only the frequency range where the e-mode grows, $0.4\Omega_{H^+} - 0.5\Omega_{H^+}$. The result is almost the same as in Figure 4 with the exception of no resonances for the pitch angles greater than about 55 degrees. So, for correct description of the RC-EMIC wave interaction, both e and He^+ modes of EMIC waves should be employed. This conclusion is important because to the best of our knowledge, in most previous modeling of the RC-EMIC wave interactions in a multi-ion plasmaspheric plasma, diffusion on the He^+-mode only has been taken into account [see, e.g., *Jordanova et al.*, 2001]. (While the above speculations seem reasonable, it is obvious that in order to check the validity of the conclusion regarding the e-mode, the RC-EMIC wave simulation including both He^+ and e modes is required. It is out of the purpose of the present study and will be considered separately.)

2.3. Numerical Schemes and Initial and Boundary Conditions

[13] To solve kinetic equation (1), *Jordanova et al.* [1996a, 1997] rewrote it in the conservative form and employed the "time splitting" method [*Yanenko*, 1971]. The advantage of the splitting method is that the multidimensional problem is split into a sequence of one-dimensional problems. For each time step we could obtain an approximate solution to the multidimensional problem by consecutively solving several one-dimensional problems using the result obtained from the previous one as the initial condition for each following problem. The order of the solution operators is reversed during the next time step to achieve second-order accuracy in time. The first-order advective terms due to drifts and Coulomb drag energy degradation are solved using a high-resolution method that combines the second order Lax-Wendroff scheme with the first-order upwind scheme via a superbee flux limiter [*LeVeque*, 1992]. Analytical solutions for the charge exchange and the atmospheric loss terms and also for the wave kinetic equation (2) are used at each time step. The pitch angle diffusion terms due to Coulomb scattering and wave-ion interaction are solved with the Crank-Nicolson scheme [e.g., *Potter*, 1973]. This scheme is an implicit algorithm which is second-order accuracy in both pitch angle and time.

[14] Equation (1) should be accompanied by the initial and boundary conditions, and equation (2) should be accompanied by the initial condition. (Note that the longi-

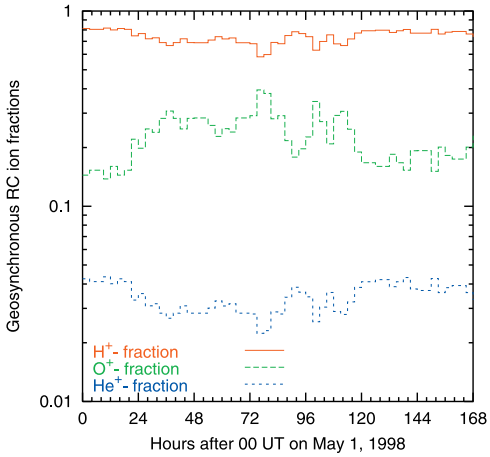

Figure 5. Fractions of the RC ions at geosynchronous distance for the 1–7 May 1998 storm period.

tudes $-\pi/2 \leq \varphi \leq \pi/2$, and $\pi/2 < \varphi < 3\pi/2$ correspond to the nightside and the dayside MLTs, respectively.) The boundary condition for F on the r coordinate axis is

$$F(r = r_{max}, t) = u(\varphi, E, \mu_0, t) \tag{7a}$$

for $-\pi/2 \leq \varphi \leq \pi/2$

$$F(r = r_{min}, t) = 0 \tag{7a$'$}$$

for $\pi/2 < \varphi < 3\pi/2$.

[15] In our model the r_{max} is close to the geostationary distance, and the nightside boundary condition, $u(\varphi, E, \mu_0, t)$, is calculated using flux measurements from the Magnetospheric Plasma Analyzer (MPA) and the Synchronous Orbit Particle Analyzer (SOPA) instruments on the geosynchronous LANL satellites during the modeled event. According to the paper by *Young et al.* [1982], we divide the total flux, measured at geostationary orbit, between H^+, O^+, and He^+ RC ions depending on geomagnetic and solar activities (as measured by Kp and $F_{10.7}$ indices). For the 1–7 May 1998 storm period the geosynchronous ion fractions are shown in Figure 5. The "φ boundary condition" reflects a periodicity of the phase space distribution function and is expressed as

$$F(\varphi = 0, t) = F(\varphi = 2\pi, t). \tag{7b}$$

For energy variable the boundary condition is set as

$$\partial F(E, t)/\partial E|_{E_{min}} = 0 \tag{7c}$$

for $-\pi/2 \leq \varphi \leq \pi/2$

$$F(E = E_{max}, t) = 0 \tag{7c$'$}$$

for $\pi/2 < \varphi < 3\pi/2$.

[16] The boundary condition for the μ_0 drift process is

$$\partial F(\mu_0, t)/\partial \mu_0|_{\mu_0=1} = 0 \tag{7d}$$

for $-\pi/2 \leq \varphi \leq \pi/2$

$$\partial F(\mu_0, t)/\partial \mu_0|_{\mu_0=0} = 0 \tag{7d$'$}$$

for $\pi/2 < \varphi < 3\pi/2$ and for the pitch angle diffusion, due to Coulomb scattering and wave-ion interaction, these conditions are

$$\left.\frac{\partial F(\mu_0, t)}{\partial \mu_0}\right|_{\mu_0=0} = 0, \qquad \left.\frac{\partial F(\mu_0, t)}{\partial \mu_0}\right|_{\mu_0=1} = 0, \tag{7e}$$

which reflect the fact of no F-fluxes through the boundaries of an available μ_0-region.

[17] To obtain the self-consistent initial conditions for equations (1) and (2), the simulation was started at 0000 UT on 1 May 1998 using background noise level for the EMIC waves [e.g., *Akhiezer et al.*, 1975], the statistically derived quiet time RC proton energy distribution of *Sheldon and Hamilton* [1993], and the initial pitch angle characteristics of *Garcia and Spjeldvik* [1985]. The RC energy distribution is constructed from measurements of the charge-energy-mass (CHEM) spectrometer on board of AMPTE/CCE satellite during the quiet conditions with $|Dst| < 11$ nT and $Kp < 2^+$. The pitch angle characteristics are derived from the quiet time radiation belt ion data of instruments flown on Explorer 45. In about 20 hours the wave magnetic energy distribution reaches a quasi-stationary state indicating that the RC-EMIC wave system achieves a quasi self-consistent state. So, the self-consistent modeling of the May 1998 storm period is started at 0000 UT on 2 May (24 hours after 1 May, 0000 UT) using solutions of the equations (1) and (2) at 2400 UT on 1 May as the initial conditions for further simulation. At this time a small region of EMIC wave activity is observed in the postnoon-dusk MLT sector with the typical wave magnetic field amplitudes of order 1 nT.

2.4. Approaches Used in Simulation

[18] The geomagnetic field, B, used in our simulation, is taken to be a dipole field. The electric field is expressed as the shielded (factor of 2) Volland-Stern-type convection field [*Volland*, 1973; *Stern*, 1975], which is Kp-dependent, and a corotation field [e. g., *Lyons and Williams*, 1984]. The plasmaspheric cold electron density, n_{e0}, is calculated with the time-dependent equatorial model of *Rasmussen et al.* [1993]. For modeling the wave-ion interaction, we also employ a 3-D model of the core plasma density of *Angerami and Thomas* [1964], which is adjusted to the Rasmussen model at the equator. Geocoronal neutral hydrogen number densities, used to calculate loss due to charge exchange, are obtained from the spherically symmetric model of *Chamberlain* [1963] with its parameters given by *Rairden et al.* [1986]. For simplicity, in present simulation the RC-EMIC wave coupling is modeled for pure electron-proton thermal plasma. Nevertheless, Coulomb collisions of the RC ions with plasmaspheric core plasma are taken into account for the electron, 77% of H^+, 20% of He^+, and 3% of O^+ thermal plasma (these proportions are in the range of 10–30% for He^+ and 1–5% for O^+, following observations by *Young et al.* [1977] and *Horwitz et al.* [1981]). An initial study of RC development during the May 1998 storm period was presented by *Farrugia et al.* [2003], who have used the RC kinetic model of *Jordanova et al.* [1998a] to model Dst variation during the storm and to calculate energy content for the major RC ion species, H^+, O^+, and He^+. They found that during this storm the energy

density of H^+ is greater than twice that of O^+ at all MLTs, and the contribution of He^+ to the RC energy content is negligible. This result allows us to assume the RC is entirely made up of energetic protons and to ignore the He^+ and O^+ RC ions in the simulation.

[19] In the present model the equatorial simulation domain is from L = 2 to L = 6.5 and covers all MLTs with resolutions $\Delta L = 0.25$ and $\Delta\varphi = 1$ hour. The energy domain is 0.01–430 keV with $(\Delta E)_1 = 0.003$ keV and $(\Delta E)_{k+1}/(\Delta E)_k = 1.36$. The phase space distribution function is assumed to be symmetric to about a 90° pitch angle, and only the range 0–90 degrees is considered. If equatorial pitch angle $\alpha_0 \geq 21.73°$ (it is loss cone boundary at L = 1.75), then the grid spacing for μ_0 is set up to $(\Delta\mu_0)_1 = 0.031$, $(\Delta\mu_0)_{l+1}/(\Delta\mu_0)_l = 0.98$. Inside of the loss cone the resolution is gradually increasing, and for $\mu_0 \approx 1$, there is $(\Delta\mu_0)_{lmax} \approx 10^{-4}$; note that μ_0-grid includes all the loss cone points corresponding to the selected L-grid. The timestep for simulation is determined from the Courant-Friedrichs-Lewy condition to be $\Delta t = 20$ s. An available angular frequency range of EMIC waves is selected to be $2\pi \times 0.5$ rad Hz $\leq \omega \leq 2\pi \times 5.5$ rad Hz, corresponding approximately to the Pc 1 frequency range, and the frequency spacing is $\Delta\nu = \Delta\omega/2\pi = 0.5$ Hz. Calculations of the EMIC wave growth rates and the wave diffusion coefficients are consuming the main part of the computational time. For example, to calculate the growth rates we have to evaluate the 2-D integrals for each time step in the 5-D grid of $(r, \varphi, \lambda, \omega, \theta)$ and in the $(r, \varphi, \lambda, E, \mu_0)$-space for calculating the diffusion coefficients. In order to decrease the calculating efforts, a few physically reasonable assumptions are introduced in the simulation. The peaks of EMIC wave growth rates take place for a field-aligned wave propagation, and the test calculations showed that for $27° \lesssim \theta$ the EMIC wave PSD is about noise level. So, in present simulation we consider the normal angle ranges of [0°, 27°] for forward and of [153°, 180°] for backward wave propagations with resolution $(\Delta\theta)_i = 4.5°$. With increasing the absolute value of magnetic latitude, λ, the EMIC wave growth rates vanish, and for $|\lambda| \approx 13°$ the growth rate values are more on an order of magnitude less than at the equator. This fact allows us just to put the growth rates to zero outside ±13° of the equator (actually, for the selected λ-grid, outside of ±13.4°).

[20] The RC-EMIC wave interaction is neglected if PSD $\langle B_{\omega,\theta}{}^2\rangle < 2 \times 10^{-4}$ nT^2/(rad^{2}Hz); for qualitative estimations this inequality may be rewritten in the term of EMIC wave magnetic field as $B_w{}^2 \ll 10^{-3}$ nT^2. Finally, the quasi-linear approach is valid if (1) the EMIC wave amplitudes are small enough in order to neglect in the series the term with a second power of the wave energy, and (2) the random phase approximation (RPA) takes place, i.e., the wave phases are random. Recently, using test particle simulations, *Kuramitsu and Hada* [2000] have shown that quasi-linear diffusion is consistent with nonlinear diffusion in RPA for the EMIC wave amplitudes of

$$\frac{B_w^2}{B^2} \lesssim 0.05, \tag{8}$$

and for $B_w{}^2/B^2 \sim 1$ the nonlinear ion diffusion is almost on an order of magnitude faster than a quasi-linear diffusion. Such anomalous speedup of the ion diffusion is due to nonresonant trapping of ions by the large-amplitude EMIC waves. Nonlinear interaction of the large amplitude EMIC waves (e.g., modulational instability which results in a generation of solitons and is described by derivative nonlinear Schrödinger equation [see, e.g., *Gamayunov and Khazanov*, 1995, and references therein]) leads to phase correlation, and in such a system the wave-ion interaction is quite different in comparison with a quasi-linear approach. In the course of a further model development, the possibilities of the strong nonlinear wave-ion interactions will be taken into account, but at present, according to equation (8), we just limit a growth of PSD $\langle B_{\omega,\theta}{}^2\rangle$ by the value 25 nT^2/(rad^{2}Hz).

3. Results and Discussions

[21] Below we present a few particular results regarding two components of the model, i.e., particle and wave components. Comparisons between the experimentally observed data and the model results are also presented, but firstly, we outline in brief the interplanetary and geomagnetic situations during the May 1998 storm.

3.1. Interplanetary Data and Geomagnetic Indices During the May 1998 Storm Period

[22] Interplanetary data for 1–7 May 1998 are obtained from the Magnetic Field Investigation (MFI) [*Lepping et al.*, 1995] and the Solar Wind Experiment (SWE) [*Ogilvie et al.*, 1995] instruments aboard the WIND satellite and are presented in detail in Figure 6. The three geomagnetic indices for the 2–7 May 1998 period are shown in Figure 7, and reflect the changes of interplanetary conditions. The interplanetary configuration of 1–7 May 1998 consists of a coronal mass ejection (CME) interacting with a trailing faster stream [*Farrugia et al.*, 2003]. The CME drives an interplanetary shock observed by the instruments aboard the WIND spacecraft at about 2220 UT on 1 May. Four episodes of the large negative north-south IMF component, B_Z, are monitored. The first episode starts at ~0400 UT on 2 May (28 hours after 1 May, 0000 UT), the second at 0230 UT on 4 May (7430 hours after 1 May, 0000 UT), and the third and fourth at ~0200 UT and ~1200 UT on 5 May (9800 and 10800 hours after 1 May, 0000 UT, respectively). These caused a "triple-dip" storm with the minimums $Dst = -106$ ($Dst^* = -75$) nT, $Dst = -272$ ($Dst^* = -195$) nT, and $Dst = -153$ ($Dst^* = -103$) nT. (The fourth episode of $B_Z < 0$ is not so strongly pronounced in *Dst*, but all the episodes are well correlated with the peaks of *Kp*.) The planetary *Kp* index reached maximum values $Kp \approx 7^-$ and $Kp \approx 9^-$ at the times when Dst minimums were recorded (see Figure 7, top and bottom). The AE index during 2–7 May 1998 is shown in the middle panel of Figure 7. Several peaks, corresponding to *Kp* peaks, are seen with a maximum $AE \approx 2340$ nT at the time when absolute maximum of *Kp* index is observed.

3.2. Comparison of Model Results With Polar/HYDRA Data

[23] During 2–7 May 1998 the Polar spacecraft crossed the RC region in the prenoon-premidnight MLT sectors, and for the purpose of a comparison we use the data from the 3-D hot

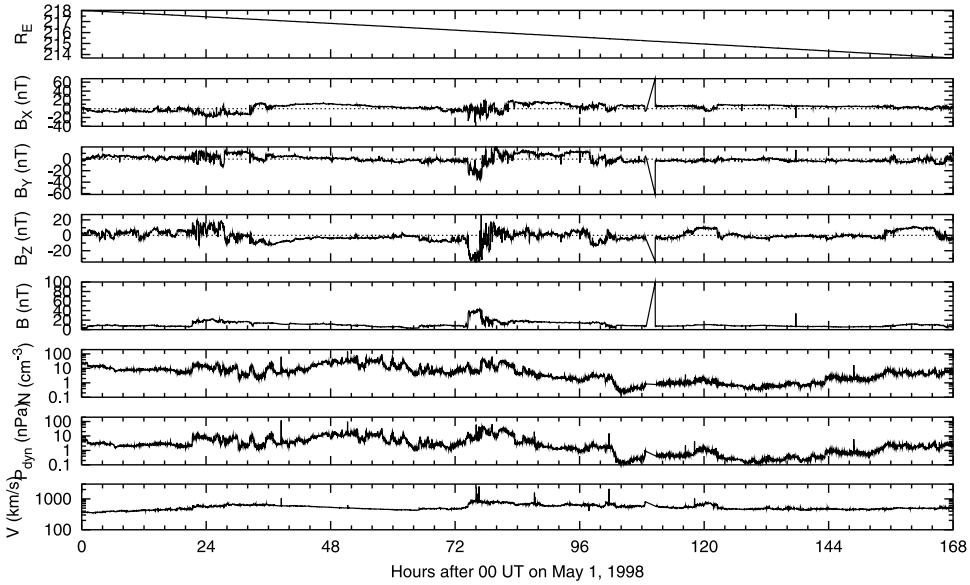

Figure 6. Interplanetary magnetic field (IMF) and solar wind parameters during a period of 1–7 May 1998 from the WIND/MFI and the WIND/SWE instruments. From the top to the bottom panels: the distance from the center of Earth, the GSM-X, -Y, and -Z components of the IMF and the IMF's magnitude, the solar wind proton number density, the ion dynamic pressure, and the solar wind bulk velocity.

plasma Polar/HYDRA instrument [*Scudder et al.*, 1995]. The HYDRA instrument is a collection of electrostatic analyzers designed for high-resolution observations of electron and ion velocity distributions covering the energy range from 18 eV to 18.5 keV. (Note that HYDRA does not provide an ion composition information and we assume all the ions to be H^+. This assumption overestimates the experimental data presented below.) The width of the HYDRA energy windows is ±6% centered at the mean energy, and the pitch angle windows are ±3.5° about the mean field of view direction.

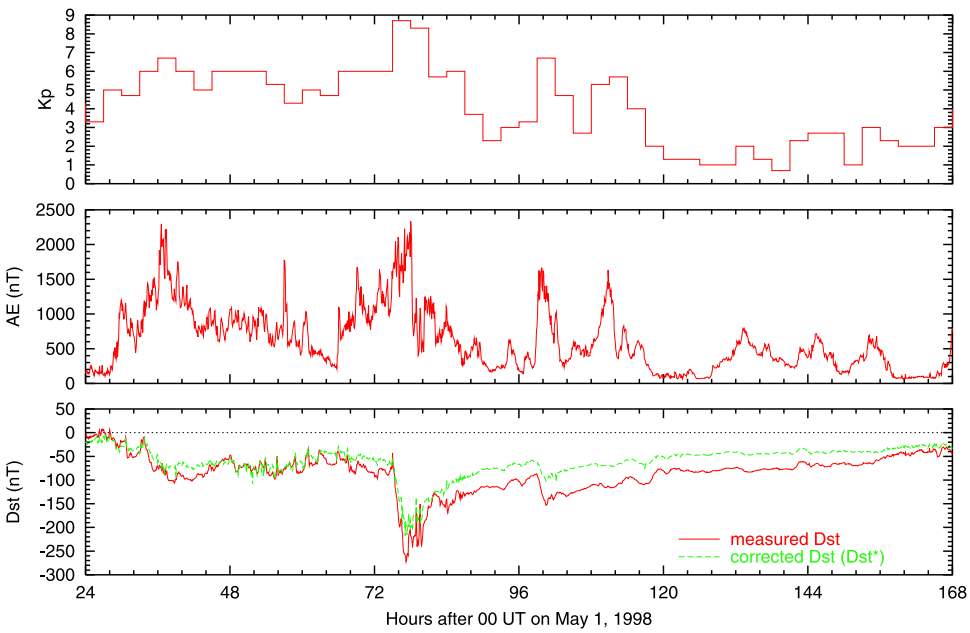

Figure 7. Geomagnetic indices for the 2–7 May 1998 storm period. (top) 3-hour *Kp* index; (middle) *AE* index which is calculated from the data of 67 stations with magnetic latitudes between 55–76 degrees; (bottom) *Dst* indices. *Dst* index is calculated after measurements from 26 stations with magnetic latitudes below 40°. *Dst** is a *Dst* index corrected for the Chapman-Ferraro current, the quiet time current, and the effect of the Earth's induction as $Dst^* = (Dst - c_1 P_{dyn}^{1/2} + c_2)/\xi$, where $c_1 = 15.8$ nT/nPa$^{1/2}$, $c_2 = 20$ nT, coefficient for the induction is $\xi = 1.5$ [e.g., *Ebihara and Ejiri*, 2000], and the 30 min time lag between WIND and Earth is adopted after *Farrugia et al.* [2003].

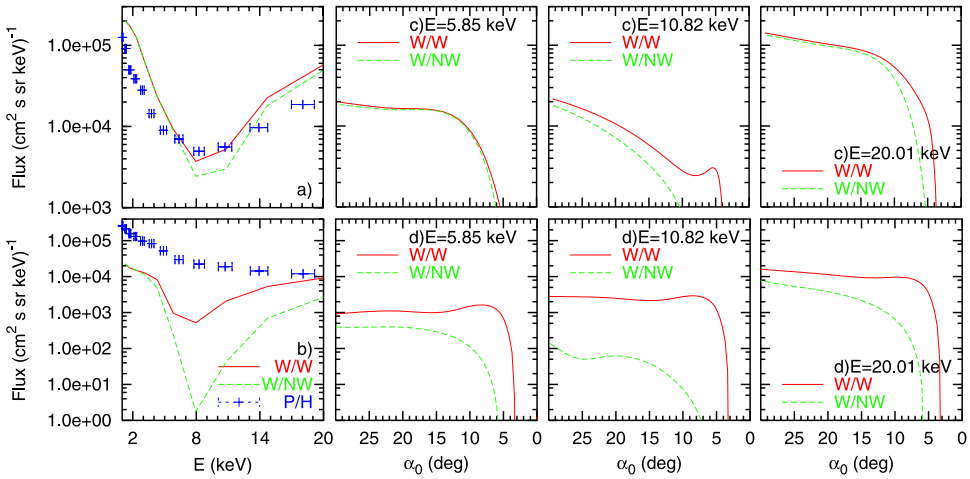

Figure 8. (a and b) Differential fluxes at the Polar spacecraft positions averaged within the bin [0°, 30°] of the local pitch angles. W/W-model results when wave-particle interaction is taken into account ("With Waves"), W/NW-model results "With No Waves", and P/H-preprocessed Polar/HYDRA data. (a) 1642 UT on 5 May 1998 (11242 hours after 1 May, 0000 UT), L = 5, MLT = 1026, λ = 19.4°. (b) 0427 UT on 7 May 1998 (14827 hours after 1 May, 0000 UT), L = 4.5, MLT = 1020, λ = 1.6°. (c and d) Equatorial pitch angle profiles which are integrated to obtain Figures 8a and 8b for three RC ion energies. Figures 8c and 8d correspond to situations in Figures 8a and 8b, respectively, except λ = 0°.

[24] The low-energy RC protons do not interact with EMIC waves and, comparing the observed data with the model results, we consider the energy range 1–18.5 keV only. In order to maximize an effect of RC-EMIC wave interaction (see Figure 5 in the paper by *Khazanov et al.* [2002]), observations inside the local pitch angle domains [0°, 30°] and [150°, 180°] are used. (In the instances considered below, the equatorial loss cone pitch angles are less than 4.7°, and the flux magnitudes decrease dramatically inside of the loss cone. So, the above pitch angle domains mainly contain the trapped fluxes. Moreover, a contribution of the loss cone ions into the HYDRA's [0°, 7°] pitch angle bin is negligible.) Also the Polar/HYDRA ion data are preprocessed as follows. (1) For each energy channel the data are averaged over the time interval $t_0 \pm \Delta t$, where $2\Delta t$ is a typical period of bounce oscillations for ~10 keV protons, then (2) the resulting data are averaged over each selected pitch angle bin, that gives "up" and "down" bounce and pitch angle averaged distribution functions, and (3) the last results are symmetrized about a 90° pitch angle as $f = (f_{\mathrm{up}} + f_{\mathrm{down}})/2$, and transferred into the differential fluxes. After the above data preprocessing, we get the data set which is ready for a comparison with the results of simulation.

[25] In the case of no parallel electric field, phase space distribution function, F, conserves along the ion trajectories, and we can easily map the equatorial ion flux to the Polar position. If λ is the geomagnetic latitude of the Polar position at time t_0, then the modeled flux, to be compared with the preprocessed Polar/HYDRA data, may be obtained as

$$J_\lambda = \frac{1}{\pi/6}\int_0^{\pi/6} \mathrm{d}\alpha j = \frac{1}{\pi/6}\int_0^{\alpha_0(\lambda)} \cdot \mathrm{d}\alpha_0 \sqrt{\frac{B(s)}{B_0}} \frac{\mu_0}{\sqrt{1-(1-\mu_0^2)B(s)/B_0}} j. \quad (9)$$

In equation (9), α and α_0 are the local and the equatorial pitch angles, respectively, j is an equatorial proton differential flux, and α_0 (λ) is defined by the equation $\alpha_0(\lambda) = \arccos\sqrt{1 - 0.25B_0/B(s)}$, where for a dipole geomagnetic field

$$\frac{B(s)}{B_0} = \frac{\sqrt{1+3\sin^2\lambda}}{\cos^6\lambda}.$$

[26] In Figure 8 we present the modeled differential fluxes along with the preprocessed Polar/HYDRA data measured in the prenoon RC region. (Bounce averaging of the HYDRA data was performed over the time period $t_0 \pm$ 60 s during which the Polar displacements do not exceed a few hundred of kilometers, which are less any spatial scales in the model.) Geomagnetic activity is culminated on 4 May (about 7715 hours after 1 May, 0000 UT), and the dayside magnetopause moves inside the geosynchronous orbit. So, both selected events refer to the late storm recovery phase during which a geomagnetic field is not so disturbed and is close to a dipole field. It follows from Figures 8a and 8b that RC-EMIC wave scattering leads to an increase in the fluxes of protons with not too little energy. This feature is more pronounced in Figure 8b, and it is due to the fact that RC-EMIC wave interaction enriches the phase space distribution function in the vicinity of the loss cone boundaries, see Figures 8c and 8d (also for details, see *Khazanov et al.* [2002]). An agreement is better for the case in Figure 8a, for which a distinction between the modeled and observed data does not exceed three times. The "HYDRA/model" ratio in Figure 8b depends strongly on proton energy and reaches 40 for the medium energies. The last comparison demonstrates very well that incorporating into the model the RC-EMIC wave scattering leads to much better agreement between the experimental data and the model results. In order to reveal the main reasons of the observed disagreement between the HYDRA measurements and the model results an additional

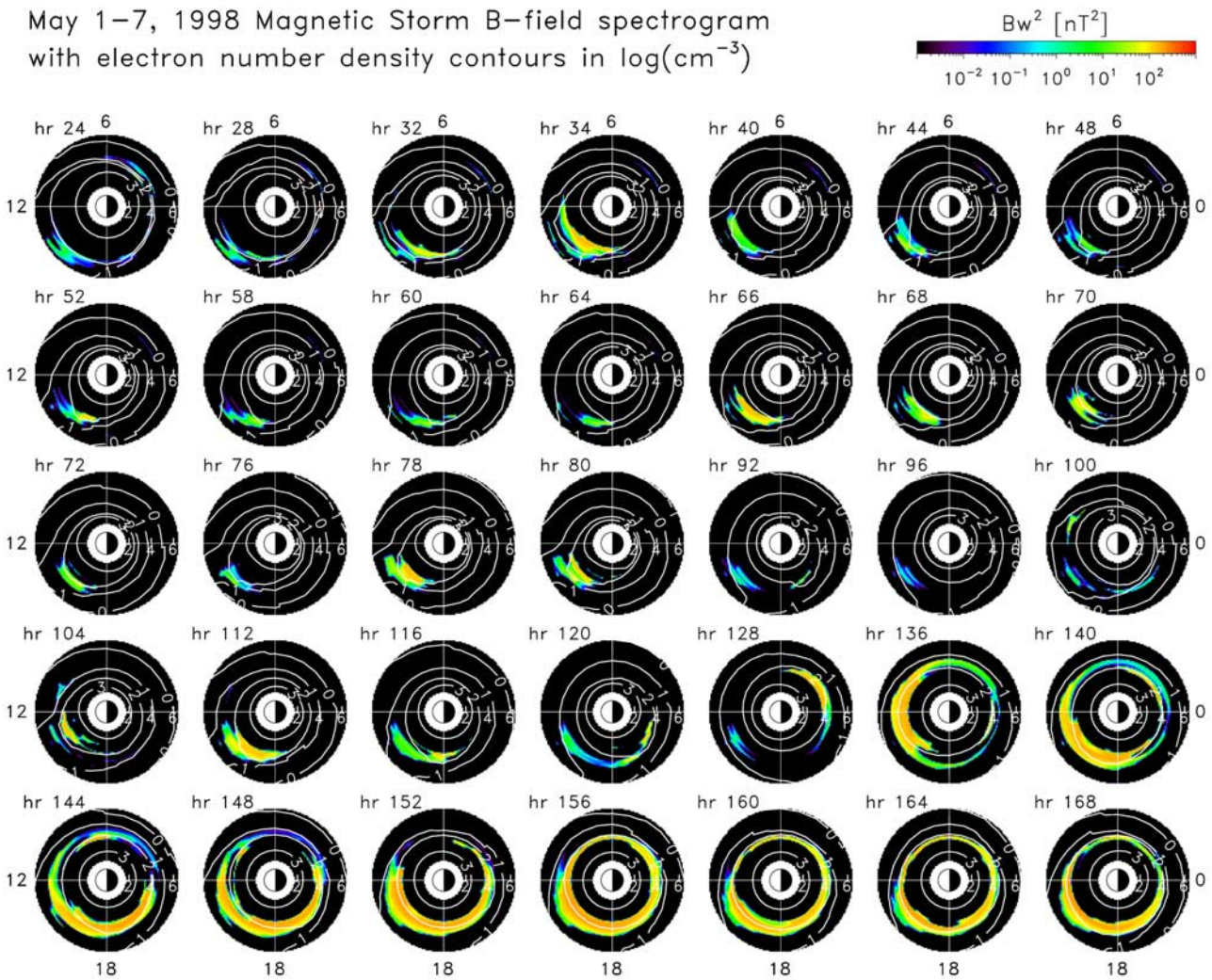

Figure 9. The (MLT, L shell) evolution of the squared EMIC wave magnetic field during the 2–7 May 1998 storm (hours are counted after 0000 UT on 1 May). White lines show contours of equatorial plasmaspheric electron density.

investigation is required. At present we believe that first, this disagreement is caused by employing a simplified model of the convection electric field because the directly observed magnetospheric electric field is noticeably different from the shielded Volland-Stern-type field [see, e. g., *Rowland and Wygant*, 1998].

3.3. EMIC Waves for 2–7 May 1998

3.3.1. Enhancement of EMIC Emission After Geomagnetic Storm

[27] In Figure 9 we present the simulated history of the 2–7 May 1998 storm period in term of EMIC wave energy and, for reference, provide the contours of the plasmaspheric electron number density. Detailed analysis of the wave active zone morphology and dynamics has been done in our previous paper [*Khazanov et al.*, 2002]. In that paper only the 4 May 1998 storm episode was analyzed; the main wave features reported by *Khazanov et al.* [2002] take place for the entire storm period. It is very interesting to demonstrate jointly with Figure 9 the modeled evolution of the pitch angle distributions for the RC protons. Not to distract from the flow of this subsubsection, we present here only one relevant figure and give a short comment. In Figure 10 the modeled pitch angle distributions of the 10.82 keV RC protons are shown for different times at L = 4 and MLT = 1500. Results both with and without wave-particle interaction are presented. Two pronounced features are observed in Figure 10. First, the growth of EMIC wave intensities causes locally the strong pitch angle diffusion which results in highly flat pitch angle distributions and filling the loss cone in comparison to the cases of no waves. Second, the observed pitch angle distributions are formed not only locally but also influenced by the wave active zones through which the RC ions were moving previously.

[28] A new pattern observed in Figure 9 is an impressive development of EMIC wave activity starting on 6 May (12000 hours after 1 May, 0000 UT), when *Kp* index is

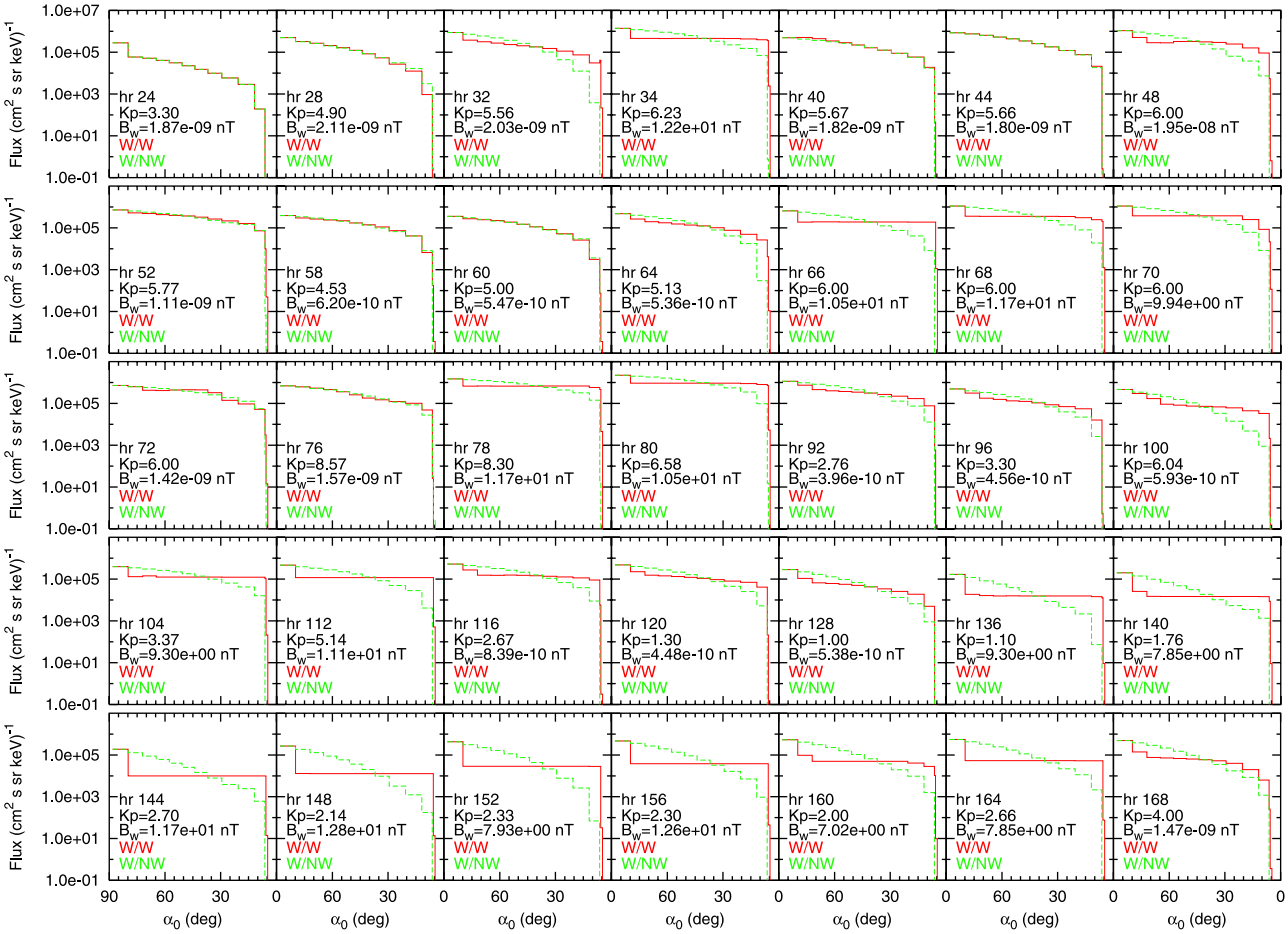

Figure 10. The modeled pitch angle distributions of the 10.82 keV RC protons for different times at L = 4 and MLT = 15 (hours are counted after 0000 UT on 1 May). Both results with (W/W) and without (W/NW) wave-particle interaction are presented, and for readability the *Kp* indices and the EMIC wave magnetic fields are provided.

practically near their absolute minimum. An enhancement of Pc 1 emissions after the main phases of geomagnetic storms has been reported for the first time by *Wentworth* [1964], who examined the records at ground-based California stations for a 3-year period from 1 August 1960 to 16 July 1963. An analysis of 25 isolated storms has allowed Wentworth to state a statistically significant result "... that 44% of the storm days, defined as day 0, were hydromagnetic active, and that the average probability that a day from 0 + 2 through 0 + 7 would be hydromagnetic active was 52% ..."; see Table 1 and Figure 3 in the paper by *Wentworth* [1964].

[29] The 2–7 May 1998 storm development is demonstrated in Figure 11 in terms of the average EMIC wave amplitudes, their peaks, and the active zone percentage. We also provide in Figure 11 the scatterplots of L shells and MLTs of B_w peaks against UT and the scatterplot of L shells against MLTs for the same wave peaks. As follows from the scatterplots, Figures 11c and 11d, the most intense EMIC waves are predominantly generated in the postnoon-premidnight MLT sector (average MLT = 15.08). However, starting at ~2000 UT on 5 May (11600 hours after 1 May, 0000 UT) the most active wave zone stably drifts eastward doing almost one and quarter of the revolutions around the Earth (see Figures 9 and 11c). After 2000 UT on 6 May (14000 hours after 1 May, 0000 UT) the most intense waves recede back to the MLTs near noon. An average L shell of the most intense EMIC waves is L = 4.16.

[30] Averaged values of B_w are derived from the wave active zones with $B_w \geq 0.1$ nT as $\langle B_w \rangle = \int_{(B_w \geq 0.1\mathrm{nT})} \mathrm{d}r\mathrm{d}\varphi r B_w / \int_{(B_w \geq 0.1\mathrm{nT})} \mathrm{d}r\mathrm{d}\varphi r$. Information, extracted from Figure 9 and summarized in Figure 11, allows us to examine in a quantitative manner the poststorm intensification of EMIC waves. It follows from Figure 11a that starting at 0200 UT on 6 May (12200 hours after 1 May, 0000 UT) the EMIC wave amplitudes stably grow being above the average magnitudes. The (MLT, L shell) extent of the wave active zone with $B_w \geq 0.1$ nT begins to increase about 24 hours earlier and reaches its average value of 11% at ~1000 UT on 6 May (13000 hours after 1 May, 0000 UT). During the major period of the storm the wave active zone occupies only a minor part of an equatorial simulation domain and does not exceed an average value of 11%, but this situation changes dramatically on 6 May (about 13000 hours after 1 May, 0000 UT) when a square of the active zone grows very sharply, maximizing at 25% in about 12 hours (see Figure 11a).

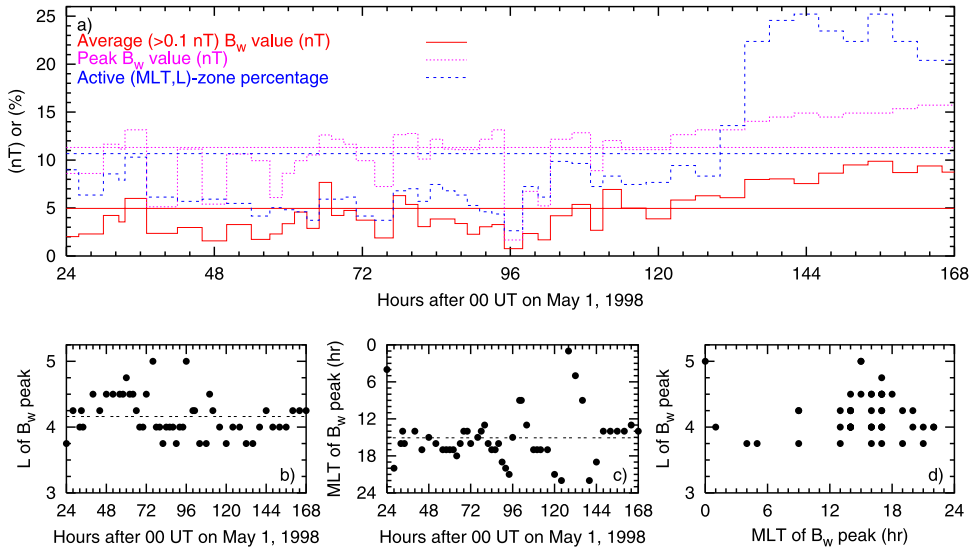

Figure 11. (a) The modeled 2–7 May 1998 storm history in the terms of EMIC wave amplitudes. Averaged B_w values are derived from the active zone with $B_w \geq 0.1$ nT. Active (MLT, L shell) zone percentage is calculated as $(\int\int_{(B_{w>0.1nT})} \mathrm{d}r\,\mathrm{d}\varphi r / \int_{L=2}^{L=6.5} \int_0^{2\pi} \mathrm{d}r\,\mathrm{d}\varphi r) \times 100\%$. (b and c) The scatterplots of L shells and MLTs of B_w peaks against UT. (d) The scatterplot of L shells versus MLTs for the peaks of B_w. Horizontal lines give the corresponding average values obtained for entire storm period as $\langle x \rangle = \int x(t)\mathrm{d}t / \int \mathrm{d}t$.

Such wave energy evolution obviously demonstrates an enhancement of EMIC wave emissions starting in about 2 days after absolute *Dst* minimum of the considered geomagnetic storm.

3.3.2. EMIC Wave Power Spectral Density

[31] It is well known that a quasi-linear wave-particle interaction strongly depends on the wave/particle characteristics, particularly on the wave PSD which itself is determined by a self-consistent evolution of the wave-particle system. In previous studies, to describe a quasi-linear interaction of EMIC waves and RC ions, a Gaussian approximation to the shape of PSD is frequently employed [e.g., *Lyons*, 1974; *Abel and Thorne*, 1998a, 1998b; *Albert*, 1999; *Jordanova et al.*, 2001]. In order to quantitatively test this assumption we examine the PSDs self-consistently generated in our model during the 2–7 May 1998 storm period. All the theoretically obtained PSD patterns are classified on the basis of their shapes. There are four classes, and an example from each class is presented in Figure 12. The first class includes the single-peaked PSDs of a symmetric shape, the second class includes double-peaked PSDs (both symmetric and asymmetric PSDs are included), and the third and the fourth classes are right-side and left-side extended the single-peaked PSDs, respectively. (Note that among about 1400 examined PSD patterns, only a few patterns could not be referred to any of the above four classes. All these "not classified" PSDs have three peaks, and we include these patterns in class number 2.) We also present in Figure 12 two different approximations to the model results. The "blue" approximations are Gaussian fits,

$$B^2(\nu) = N \exp\left\{-\frac{(\nu - \langle\nu\rangle)^2}{2D_\nu}\right\},$$

with moments N, $\langle\nu\rangle$, and D_ν as follows from the model obtained PSDs, and the "green" fits are produced by connecting the consecutive points with natural cubic splines. We can state that for all four PSD classes the spline approximations are much better fits to the histograms than the Gaussian curves. It is also obvious that a Gaussian approximation does not reproduce the asymmetric data well (see Figures 12b–12d) because a Gaussian curve is a symmetric one, and it cannot fit the data well with an essential asymmetry.

[32] Figure 12 demonstrates only the shapes of the modeled PSDs, but it does not provide us with information on how frequently each PSD class occurs during storm development. In order to obtain the occurrence rates for the four presented PSD classes, we select only the patterns of PSDs which satisfy criterion $B_\nu^2 \geq 1$ nT^2/Hz (such values of PSDs are consistent with the AMPTE/CCE observations of Pc 1–2 [*Anderson et al.*, 1992a, 1992b]). There are 1368 patterns for the entire 2–7 May 1998 storm period. Some statistical results are presented in Figure 13 after processing the selected PSDs. The first class of PSDs is represented by 35.09% of the total patterns, and the fourth, third, and second classes by 25.88, 21.78, and 17.25 percent, respectively. The averaged occurrence rates, obtained for the entire storm period as $\langle x \rangle = \int x(t)\,\mathrm{d}t / \int \mathrm{d}t$, are drawn by horizontal lines in Figure 13. There are 0.75, 0.43, 0.52, and 0.59 percent from the top to the bottom panels, respectively. During the major part of the storm, occurrence rates for the classes 2–4 only sometimes exceed the average values for short time periods (of course, that is in comparison with the duration of the entire storm). At the same time, the class one occurrence rate is only rarely below ~0.5%, which is a typical magnitude of the average occurrence rates for classes 2, 3, and 4. So, as follows from Figure 13, the occurrence rate of the first class PSDs dominates practically all the time for more than 4 days after 1 May. The situation is qualitatively changing on 6 May (12000 hours after 1 May, 0000 UT). The occurrence rates in all PSD classes grow (not starting simultaneously), but the peak values in classes 2(3) and 4 are two and one and a half times higher, respectively,

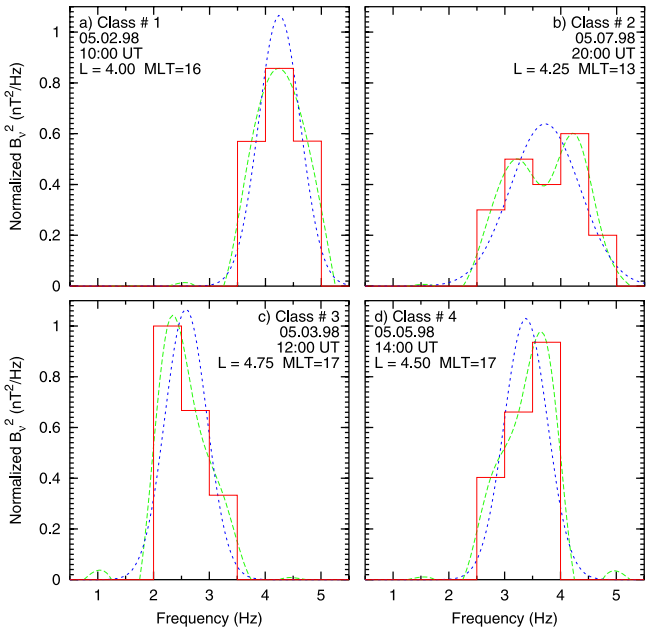

Figure 12. Examples for the four classes of PSD histograms as follows from our simulation the 2–7 May 1998 storm period (red lines). All the PSDs are normalized to 1 nT^2, so only the shapes of PSDs are demonstrated. Two approximations to the model results are also provided. There are Gaussian fits (blue lines), and the fits produced by connecting the consecutive points with natural cubic splines (green lines).

than in class one. As we can see from Figure 13, the total periods during which the classes 2–4 dominate the class one are about 20 hours for each of them, and these periods take place at different times. So, in about 2 days after the storm main phase on 4 May (about 7715 hours after 1 May, 0000 UT), mainly non-Gaussian PSDs of EMIC waves are observed along with a reappearance of the strong EMIC wave emissions.

4. Conclusions

[33] In this paper we have presented for the first time a complete description of the model of magnetospheric RC ions self-consistently interacting with generated EMIC waves. This model describes generation, evolution, and damping of the waves in the Earth's magnetosphere along with the RC dynamics. The model is based on a system of two kinetic equations in a quasi-linear approach; one equation describes the RC ion dynamics and another equation describes EMIC wave evolution. In previous paper ([*Khazanov et al.*, 2002]) a self-consistent model of interacting waves and ions has only been shortly outlined, and discussions of many model related details have been postponed up to the current study. For example, we have described here a new algorithm for the numerical finding of the resonant numbers for quasi-linear wave-particle interaction and have argued that correct description of a quasi-linear RC-EMIC wave interaction in a multi-ion thermal plasma should employ both e and He^+ modes of the EMIC waves.

[34] In addition to a discussion of the issues regarding the model itself, we have employed the developed model to simulate the 2–7 May 1998 geomagnetic storm. As compared with the results discussed by *Khazanov et al.* [2002], in the present study we have simulated the entire storm period and mainly have paid attention to comparisons of the obtained theoretical wave and ion data with the experimentally observed data. First, measurements of the 3-D hot plasma instrument HYDRA on board the Polar satellite have been compared with simulated number fluxes of the RC protons. In order to maximize the effect of RC-EMIC wave interaction, the Polar/HYDRA observations inside the local pitch angle domains [0°, 30°] and [150°, 180°] have been used. Second, EMIC waves have been examined from the point of view of a very interesting effect reported by *Wentworth* [1964], who has observed an essential enhancement of Pc 1 emissions in a few days after the main phases of geomagnetic storms. For theoretical studying this phenomenon, the (MLT, L shell) distributions of EMIC waves have been produced and investigated during storm progress. Finally, it is well known that a quasi-linear interaction of EMIC waves and RC ions depends on the wave/particle characteristics, particularly on the wave PSD which itself is determined by self-consistent evolution of the wave-particle system. Frequently, a Gaussian approximation to the shape of PSD is assumed for not self-consistent modeling of a quasi-linear interaction. In order to quantitatively test this assumption we have examined the theoretical shapes and the occurrence rates of PSDs self-consistently generated during the storm. Presented results of the simulation can be summarized as follows.

[35] 1. The modeled fluxes of the RC protons reproduce the Polar/HYDRA data reasonably well. One of the presented comparisons demonstrates that incorporating in model the RC-EMIC wave scattering leads to much better agreement between the experimental data and the model results. In order to reveal the main reason(s) of observed disagreement between the Polar/HYDRA measurements and the model results an additional investigation is required. At present we believe that the main reason for this disagreement is due to a simplified model of the used convection electric field.

[36] 2. In about 2 days after absolute *Dst* minimum of the modeled storm a stable growth of the EMIC wave amplitudes rises above the average magnitudes. The (MLT, L shell) extent of the wave active zone, $B_w \geq 0.1$ nT, begins to increase about 24 hours earlier and reaches an average value of 10.7% at ~1000 UT on 6 May 1998 (13000 hours after 1 May, 0000 UT). During the major part of the storm period the wave active zone occupies only a minor part of the equatorial simulation domain and does not exceed an average value of 10.7%. This situation is strongly changing on 6 May when the square of the wave active zone grows very sharply maximizing at 25.2% in about 12 hours.

[37] 3. All the patterns of self-consistently generated PSDs may be classified on the basis of their shapes. There are four classes that are found. The first class includes the single-peaked PSDs of a symmetric shape, the second class includes double-peaked PSDs (both symmetric and asymmetric PSDs are included), and the third and the fourth classes are right-side and left-side extended the single-peaked PSDs, respectively. For all PSD classes the spline approximations are much better fits to the histograms than the Gaussian curves.

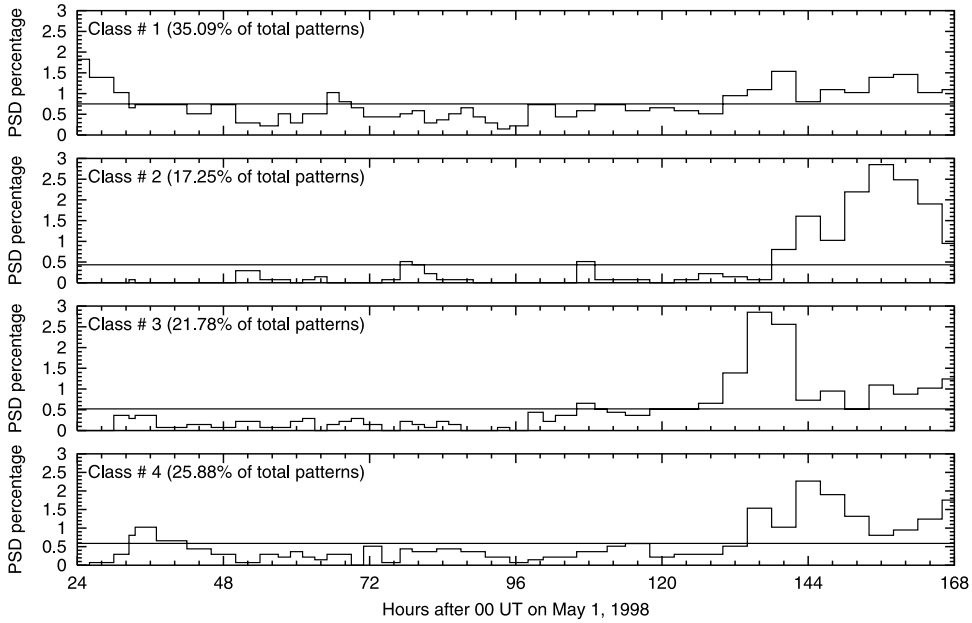

Figure 13. Occurrence rates of the four PSD classes during the 2–7 May 1998 storm. Horizontal lines represent the corresponding average values obtained for entire storm period.

[38] 4. During the storm, the first class of PSDs is represented by 35.09% of the total patterns, and the fourth, third, and the second classes by 25.88, 21.78, and 17.25 percent, respectively. The averaged occurrence rates, obtained for the entire storm period, are 0.75, 0.43, 0.52, and 0.59 percent for the first through fourth classes, respectively. The occurrence rate of the first class PSDs dominates almost all the time during more than four days after 1 May. Starting on 6 May (12000 hours after 1 May, 0000 UT), the occurrence rates for all PSD classes enhance essentially, and the peak values in classes 2(3) and 4 are two and one and a half times higher than in class one, respectively. Total periods during which the classes 2–4 dominate the class one are about 20 hours for each of them, and these periods take place at different times (see Figure 13). So, in about two days after the main storm phase on 4 May (about 7715 hours after 1 May, 0000 UT), mainly 2–4 classes of the PSDs are observed.

Appendix A: Terms in Equations (1) and (2)

[39] The drift and the loss terms in equation (1) are derived by *Jordanova et al.* [1994, 1996a, 1997], and are given below for completeness.

A1. Drift Velocities in Equation (1)

[40] The bounce-averaged radial and azimuthal drift velocities are

$$\left\langle \frac{dr}{dt} \right\rangle = -\frac{Ar^4 \cos\varphi}{M}, \tag{A1}$$

$$\left\langle \frac{d\varphi}{dt} \right\rangle = \frac{C + 2Ar^3 \sin\varphi}{M} - \frac{3Er}{Z|e|M}\left(1 - \frac{I(\mu_0)}{6h(\mu_0)}\right). \tag{A2}$$

Where $C = 5.84 \times 10^{11}$ V m, and determines a corotation electric field. Convection electric field is assumed to be Kp-dependent, and for the factor A we use the expression empirically determined by *Maynard and Chen* [1975] as

$$A = \frac{1.11 \times 10^{-12}}{(1 - 0.16Kp + 0.01Kp^2)^3}\,\mathrm{Vm}^{-2}.$$

$M = 8.02 \times 10^{15}$ Tm^3 is a dipole moment of the Earth, $Z|e|$ is an electric charge of the RC ions, and the functions $h(\mu_0)$ and $I(\mu_0)$ [*Ejiri*, 1978] are defined by

$$h(\mu_0) = \frac{1}{r}\int_0^{\lambda_m} \frac{\mathrm{ds}}{\sqrt{1 - B(s)/B_m}} \quad I(\mu_0) = \frac{2}{r}\int_0^{\lambda_m} \mathrm{ds}\sqrt{1 - B(s)/B_m},$$

where $B(s)$ and B_m are the intensities of geomagnetic field at the current position, s, and at the mirror latitude, λ_m, and ds is an element along magnetic field line.

[41] The bounce-averaged rates of change of kinetic energy and the cosine of the equatorial pitch angle for RC ions are

$$\left\langle \frac{d\mu_0}{dt} \right\rangle = -\frac{(1 - \mu_0^2)Ar^3 \cos\varphi I(\mu_0)}{4\mu_0 M h(\mu_0)}, \tag{A3}$$

$$\left\langle \frac{dE}{dt} \right\rangle = \frac{3EAr^3 \cos\varphi}{M}\left(1 - \frac{I(\mu_0)}{6h(\mu_0)}\right). \tag{A4}$$

A2. Loss Terms in Equation (1)

A2.1. Charge Exchange Loss

[42] The charge exchange of the RC ions with neutral hydrogen from the geocorona results in a generation of the high energy neutrals and low energy protons. The bounce-averaged change of the phase space distribution function due to the charge exchange loss is expressed as

$$\left\langle \left(\frac{\delta F}{\delta t}\right)_{ce} \right\rangle = -\sigma_H v \langle n_H \rangle F, \tag{A5}$$

where σ_H is a charge exchange cross section of the RC ion species and neutral hydrogen, v is a velocity of the RC ion, and $\langle n_H \rangle$ is the bounce-averaged number density of the neutral hydrogen. In the present study the spherically symmetric model of *Chamberlain* [1963] with its parameters given by *Rairden et al.* [1986] is employed in order to obtain the neutral hydrogen number density $\langle n_H \rangle$ (for details see [*Schulz and Blake*, 1990]). The charge exchange cross section is used from *Barnett* [1990] or *Phaneuf et al.* [1987] depending on H^+/He^+ or O^+ RC ions are under modeling.

A2.2. Coulomb Collisions With Core Plasma

[43] Coulomb interactions of the RC ions with plasmaspheric thermal electrons and ions lead to energy degradation and to pitch angle scattering of the RC ions. These processes are described by the Fokker-Planck equation [e.g., *Hinton*, 1983]. After bounce-averaging, the change of the RC phase space distribution function due to Coulomb collisions is described as

$$\left\langle \left(\frac{\delta F}{\delta t}\right)_{cc} \right\rangle = \frac{1}{\sqrt{E}} \frac{\partial}{\partial E} \left(\sqrt{E} \left\langle \left(\frac{dE}{dt}\right)_{cc} \right\rangle F \right) + \frac{1}{\mu_0 h(\mu_0)} \frac{\partial}{\partial \mu_0} \left(\mu_0 h(\mu_0) \langle D_{cc} \rangle \frac{\partial F}{\partial \mu_0} \right), \tag{A6}$$

where

$$\left\langle \left(\frac{dE}{dt}\right)_{cc} \right\rangle = \sqrt{2E}\Gamma m^{3/2} \sum_b \frac{\langle n_b \rangle Z_b^2}{kT_b} G\left(\frac{v}{v_b}\right), \tag{A7a}$$

$$\langle D_{cc} \rangle = \frac{(1-\mu_0^2)\Gamma}{2\mu_0^2 v^3} \sum_b Z_b^2 \left[\Phi\left(\frac{v}{v_b}\right) - G\left(\frac{v}{v_b}\right) \right] \left\langle \frac{n_b B_0 \mu^2}{B(s)} \right\rangle, \tag{A7b}$$

$$\Gamma = \frac{Z^2 e^4 \ln \Lambda}{4\pi\varepsilon_0^2 m^2}, \tag{A7c}$$

$$G(x) = \frac{\Phi(x) - x\Phi'(x)}{2x^2}, \tag{A7d}$$

and summation should be done over the core plasma species, b. In the above equations, $Z|e|$ and $Z_b|e|$ are the charges of the RC ions and the core plasma species, respectively, and m is a mass of the RC ions; n_b is a number density of b species core plasma particles; k is a Boltzmann constant; Φ is an error function; $\ln \Lambda$ is the Coulomb logarithm; ε_0 is the permittivity of free space; $\mu = \cos \alpha$ is the cosine of the local pitch angle; B_0 is an equatorial geomagnetic field, and T_b is a temperature of b species core plasma particles with a thermal velocity $v_b = \sqrt{2kT_b/m_b}$.

[44] In order to derive the simple analytical expressions for equations (A7a) and (A7b), we assume $n_b(s)/B(s)$ to be a constant along geomagnetic field line. This assumption allows us to write the bounce-averaged expressions in the forms

$$\langle n_b \rangle = \frac{n_{b0}}{1-\mu_0^2} \left(1 - \frac{I(\mu_0)}{2h(\mu_0)} \right), \tag{A8a}$$

$$\left\langle \frac{n_b B_0 \mu^2}{B(s)} \right\rangle = \frac{n_{b0} I(\mu_0)}{2h(\mu_0)}, \tag{A8b}$$

where n_{b0} is an equatorial number density of the core plasma species. In the present simulation the plasmaspheric cold electron density, n_{e0}, is calculated with the time-dependent equatorial model of *Rasmussen et al.* [1993]. The core plasma is assumed to consist of H^+, He^+, O^+ ions with the ratios to electron density 0.77, 0.20, and 0.03, respectively, which are in the range of 0.1–0.3 for He^+ and 0.01–0.05 for O^+ following observations by *Young et al.* [1977] and *Horwitz et al.* [1981]. The temperatures of core electrons and ions are assumed to be 1 eV.

A2.3. Ion-Wave Scattering

[45] Quasi-linear interaction of the RC ions with EMIC waves mainly causes pitch angle diffusion. (The energy diffusion due to wave-particle interaction has a smaller rate due to the smaller diffusion coefficient, and we neglect this process in the present study.) Bounce-averaged change of the phase space distribution function due to quasi-linear interaction of the RC ions and EMIC waves is expressed as [e.g., *Lyons and Williams*, 1984]

$$\left\langle \left(\frac{\delta F}{\delta t}\right)_{iw} \right\rangle = \frac{1}{\mu_0 h(\mu_0)} \frac{\partial}{\partial \mu_0} \left(\mu_0 h(\mu_0) \langle D_{iw} \rangle \frac{\partial F}{\partial \mu_0} \right). \tag{A9}$$

In equation (A9) a bounce-averaged diffusion coefficient has the form:

$$\langle D_{iw} \rangle = \frac{1-\mu_0^2}{h(\mu_0)\mu_0^2 v^2} \int_0^{\lambda_m} d\lambda D_{\alpha\alpha} \cos\alpha \cos^7 \lambda, \tag{A10}$$

where integration should be done along a geomagnetic field line (λ is a geomagnetic latitude). The local pitch angle diffusion coefficient, $D_{\alpha\alpha}$, is well known and can be found in many plasma physics monographs or papers [e.g., *Lyons and Williams*, 1984]. Quasi-linear interaction is a resonance process, and diffusion coefficient $D_{\alpha\alpha}$ strongly (or even dramatically) depends on such assumed characteristics as energy, pitch angle, charge and mass of the RC particle, wave frequency, normal angle, polarization, energy and

form of PSD. In order to describe the dispersive properties of EMIC waves, in the present model we employ a cold plasma approximation [e.g., *Stix*, 1962] for a core plasmaspheric plasma of electrons, H^+, He^+, and O^+.

A2.4. Atmospheric Loss

[46] The RC ions with pitch angles inside of the equatorial loss cone have the mirror points inside dense atmosphere. This fact leads to the emptying of a loss cone twice per bounce period τ_B. The bounce-averaged change of the phase space distribution function due to atmospheric loss may be described as [*Lyons and Williams*, 1984]

$$\left\langle \left(\frac{\delta F}{\delta t}\right)_{atm} \right\rangle = -\frac{F}{\tau_{atm}}, \tag{A11}$$

where a typical time for the leakage into the atmosphere is

$$\tau_{atm} = \begin{cases} \tau_B/2, & \text{for } \alpha_0 \text{ in the loss cone} \\ \infty, & \text{for } \alpha_0 \text{ out of the loss cone} \end{cases}$$

and

$$\tau_B = \frac{4}{v}\int_0^{\lambda_m} \frac{\mathrm{ds}}{\sqrt{1 - B(s)/B_m}} = \frac{4rh(\mu_0)}{v}.$$

In the model an altitude of 200 km is adopted as an upper boundary of the dense atmosphere. Note that in writing equation (A11) we neglected the collisional variation of F down from the upper atmosphere boundary.

A3. Nonideal Terms in Equation (2)

A3.1. Reflection Coefficient

[47] The EMIC waves propagate along geomagnetic field lines and reflect at the ionosphere altitudes. Owing to nonideal reflection from the ionosphere part of the wave energy will be lost during reflection, and this loss is described in equation (2) by an effective reflection coefficient R. In our model we employ the expression for EMIC wave reflection coefficient which was obtained by *Lyatsky and Maltsev* [1983]. (The idea how to obtain reflection coefficient and some particular results can be also found, for example, in the papers by *Knudsen et al.* [1992], *Belyaev and Polyakov* [1980].) To derive reflection coefficient *Lyatsky and Maltsev* [1983] have used the following model: plane Earth as an ideal conductor, vacuum interval, an optically thin conductive layer, and homogeneous magnetosphere. The reflection coefficient depends on both wave and ionosphere parameters and may be presented in the form

$$\mathrm{R}_{1/2} = \left|\left(\frac{N - N_{eff}}{N + N_{eff}}\right)\right|^2, \tag{A12a}$$

where N is an EMIC wave refractive index, and

$$N_{eff} = \frac{4\pi}{c}\Sigma_P - i\frac{\omega\cot\left(h\sqrt{k_0^2 - k_\perp^2}\right)}{c\sqrt{k_0^2 - k_\perp^2}} + \frac{\left(\frac{4\pi}{c}\Sigma_H\right)^2}{\frac{4\pi}{c}\Sigma_P + \frac{c}{\omega}\left(\sqrt{k_\parallel^2 - k_\perp^2} + i\sqrt{k_0^2 - k_\perp^2}\cot\left(h\sqrt{k_0^2 - k_\perp^2}\right)\right)}. \tag{A12b}$$

In equation (A12b), c is speed of light, and i is an imaginary unit; ω, $k_\parallel$, $k_\perp$ are EMIC wave frequency and components of the wave normal vector along and transverse to the ambient magnetic field, respectively, and $k_0 = \omega/c$; h is an altitude of the effective reflection layer (for practical purposes, we are treating it as the lower boundary of the ionosphere, and in the model $h = 200$ km is adopted); Σ_P and Σ_H are the height integrated Pedersen and Hall conductances, respectively. In the present simulation we adopted the analytical conductivity models of both Pedersen and Hall conductances [*Simons et al.*, 1985], which are based on 4 years of measurements of precipitating particle fluxes from Atmosphere Explorer C and D. In our model a south-north symmetry for magnetosphere is assumed. So, the total reflection index in equation (2) is just a square of the index in equation (A12a), i.e.,

$$\mathrm{R} = \left(\mathrm{R}_{1/2}\right)^2. \tag{A12c}$$

In Figure A1 we present the frequency profiles of the employed reflection index (actually its power, $\mathrm{R}^{1/4}$) to demonstrate dependencies on the governing parameters.

[48] The effects of ionospheric number density profiles on EMIC wave reflection index, and on the wave structures in the reflecting layer and on the ground were investigated in the papers [*Knudsen et al.*, 1992; *Lessard and Knudsen*, 2001; *Lysak*, 1999]. The role of the heavy plasmaspheric ions for the tunneling, reflection and absorption of EMIC waves has been discussed by *Johnson and Cheng* [1999]. Note that the effects of He^+, and O^+ plasmaspheric ions are included in our model, but in present first simulation the EMIC wave dynamics is modeled for simplicity in pure electron-proton thermal plasma.

A3.2. Growth and Damping Rates

[49] The resonating interaction of EMIC waves and plasma is described by the term γ, which includes both the wave growth and the damping. A general expression for γ is derived in many plasma physics monographs [e.g., *Lyons and Williams*, 1984] and, after omitting simple algebra, can be written as

$$\gamma_{RC} = \frac{4\pi^2\omega_{pe}^2 m_e B(s)}{\omega n_e B_0}\sum_{n,j} Z_j^2 \int_0^\infty \mathrm{d}p p^2 \frac{\Theta_{n,j,\mathbf{k}}}{32\pi W_{\mathbf{k}}}\left(\frac{\omega}{k_\parallel}\frac{\partial F_j}{\partial p} + \frac{\mu B_0}{m_j \mu_0 B(s)}\frac{\partial F_j}{\partial \mu_0} - \frac{\omega\mu^2 B_0}{k_\parallel p \mu_0 B(s)}\frac{\partial F_j}{\partial \mu_0}\right)\left(1 - \mu_0^2\right)\Bigg|_{\mu = \left(\omega - n\Omega_j\right)/\left(k_\parallel v\right)}, \tag{A13}$$

where summation should be done over RC species, j, and resonating numbers, n; $\omega_{pe}^2 = 4\pi n_e e^2/m_e$; p is a RC ion momentum, and Ω_j is a gyrofrequency of the species j RC ions. The factor $\Theta_{n,j,\mathbf{k}}/(32\pi W_{\mathbf{k}})$ depends on both RC ion characteristics and dispersive properties of plasma. This factor is cumbersome and we do not provide it here, but it can be found in the work of *Lyons and Williams* [1984].

[50] The damping rate due to interaction of EMIC waves and plasmaspheric core plasma, γ_{core}, can be easily obtained from equation (A13) for the particular phase space distribution functions F_j (in this case j marks a core plasma species). And in equation (2) the imaginary part of the wave frequency is expressed as

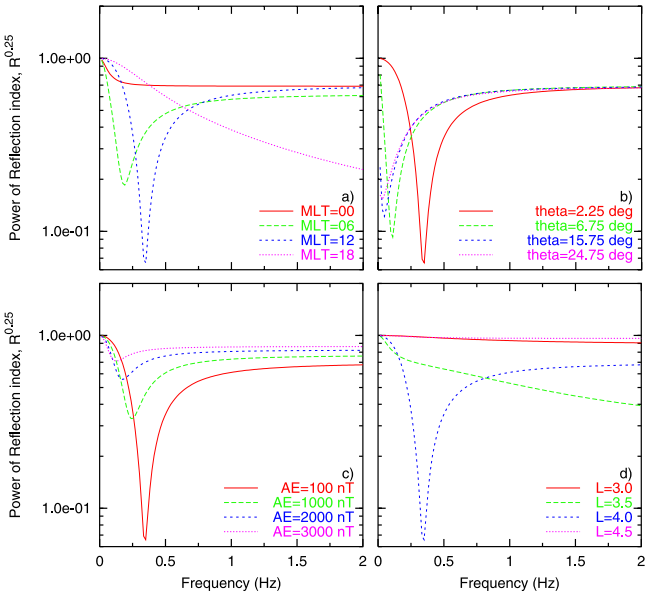

Figure A1. Power of the reflection coefficient, $R^{1/4}$, versus frequency as the functions of local time, incident wave normal angle (θ), *AE* index, and L shell. In all the plots unchangeable parameters are MLT = 1200, θ = 2.25 deg, *AE* = 100 nT, and L = 4. Pedersen and Hall conductances (mho) are (a) 0.97, 0.00; 0.30, 0.62; 0.14, 0.51; 0.06, 0.15 for MLT = 0000, MLT = 0600, MLT = 1200, and MLT = 1800, respectively; (b) 0.14, 0.51; (c) 0.14, 0.51; 0.27, 0.68; 0.50, 0.93; 0.86, 1.24 for *AE* = 100, *AE* = 1000, *AE* = 2000, and *AE* = 3000 nT, respectively; (d) 0.004, 0.02; 0.05, 0.20; 0.14, 0.51; 0.14, 0.51 for L = 3.0, L = 3.5, L = 4.0, and L = 4.5, respectively.

$$\gamma = \gamma_{RC} + \gamma_{core}.$$

In the present study we consider the core plasma to be Maxwellian with a temperature of 1 eV, and approximation of the small Larmor radius is also used.

[51] **Acknowledgments.** We would like to thank J. Scudder for providing Polar/HYDRA data, M. Thomsen and G. Reeves for providing LANL data, and P. Sloan for generating Figure 9. We are also grateful to E. Krivorutsky for useful discussions. The solar wind magnetic field and plasma data are obtained from the CDAWeb maintained by the MFI team (R. Lepping, PI) and the SWE team (K. Ogilvie, PI) of the Wind satellite. This work was supported by the National Science Foundation (NSF) grants ATM-9800830, and ATM-0101095, and the National Aeronautics and Space Administration (NASA) grant NAG5-6976.

[52] Arthur Richmond thanks Jay M. Albert and another reviewer for their assistance in evaluating this paper.

References

Abel, B., and R. M. Thorne, Electron scattering loss in Earth's inner magnetosphere: 1. Dominant physical processes, *J. Geophys. Res.*, *103*, 2385, 1998a.

Abel, B., and R. M. Thorne, Electron scattering loss in Earth's inner magnetosphere: 2. Sensitivity to model parameters, *J. Geophys. Res.*, *103*, 2397, 1998b.

Akhiezer, A. I., I. A. Akhiezer, R. V. Polovin, A. G. Sitenko, and K. N. Stepanov, *Plasma Electrodynamics*, vol. 2, Pergamon, New York, 1975.

Albert, J. M., Analysis of quasi-linear diffusion coefficients, *J. Geophys. Res.*, *104*, 2429, 1999.

Anderson, B. J., R. E. Erlandson, and L. J. Zanetti, A statistical study of Pc 1–2 magnetic pulsations in the equatorial magnetosphere: 1. Equatorial occurrence distributions, *J. Geophys. Res.*, *97*, 3075, 1992a.

Anderson, B. J., R. E. Erlandson, and L. J. Zanetti, A statistical study of Pc 1–2 magnetic pulsations in the equatorial magnetosphere: 2. Wave properties, *J. Geophys. Res.*, *97*, 3089, 1992b.

Angerami, J. J., and J. O. Thomas, Studies of planetary atmospheres: 1. The distribution of ions and electrons in the earth's exosphere, *J. Geophys. Res.*, *69*, 4537, 1964.

Barnett, C. F., Atomic data for fusion, vol. 1, Collisions of *H*, H_2, *He* and *Li* atoms and ions with atoms and molecules, *Tech. Rep. ORNL-6086/VI*, Oak Ridge Natl. Lab., Oak Ridge, Tenn., 1990.

Belyaev, P. P., and S. V. Polyakov, Boundary conditions for MHD waves at the ionosphere, *Geomagn. Aeron.*, *20*, 442, 1980.

Bespalov, P. A., and V. Y. Trakhtengerts, Cyclotron instability of the Earth radiation belts, *Rev. Plasma Phys.*, vol. 10, edited by M. A. Leontovich, Consult. Bur., New York, 1986.

Bezrukikh, V. V., and K. I. Gringauz, The hot zone in the outer plasmasphere of the Earth, *J. Atmos. Terr. Phys.*, *38*, 1085, 1976.

Bräysy, T., K. Mursula, and G. Marklund, Ion cyclotron waves during a great magnetic storm observed by Freja double-probe electric field instrument, *J. Geophys. Res.*, *103*, 4145, 1998.

Chamberlain, J. W., Planetary corona and atmospheric evaporation, *Planet. Space Sci.*, *11*, 901, 1963.

Cornwall, J. M., Cyclotron instabilities and electromagnetic emission generation mechanisms, *J. Geophys. Res.*, *69*, 4515, 1964.

Cornwall, J. M., Cyclotron instabilities and electromagnetic emission in the ultra low frequency and very low frequency ranges, *J. Geophys. Res.*, *70*, 61, 1965.

Cornwall, J. M., F. V. Coroniti, and R. M. Thorne, Turbulent loss of ring current protons, *J. Geophys. Res.*, *75*, 4699, 1970.

Cornwall, J. M., F. V. Coroniti, and R. M. Thorne, Unified theory of SAR arc formation at the plasmapause, *J. Geophys. Res.*, *76*, 4428, 1971.

Denton, R. E., M. K. Hudson, and I. Roth, Loss-cone-driven ion cyclotron waves in the magnetosphere, *J. Geophys. Res.*, *97*, 12,093, 1992.

Ejiri, M., Trajectory traces of charged particles in the magnetosphere, *J. Geophys. Res.*, *83*, 4798, 1978.

Erlandson, R. E., and A. J. Ukhorskiy, Observations of electromagnetic ion cyclotron waves during geomagnetic storms: Wave occurrence and pitch angle scattering, *J. Geophys. Res.*, *106*, 3883, 2001.

Farrugia, C. J., et al., Large-scale geomagnetic effects of May 4, 1998, *Adv. Space Res.*, *31/4*, 1111, 2003.

Gamayunov, K. V., and G. V. Khazanov, Influence of hot anisotropic ions on properties of nonlinear Alfvén waves, *Plasma Phys. Controlled Fusion*, *37*, 1095, 1995.

Garcia, H. A., and W. N. Spjeldvik, Anisotropy characteristics of geomagnetically trapped ions, *J. Geophys. Res.*, *90*, 347, 1985.

Gendrin, R., M. Ashour-Abdalla, Y. Omura, and K. Quest, Linear analysis of ion-cyclotron interaction in a multicomponent plasma, *J. Geophys. Res.*, *89*, 9119, 1984.

Gomberoff, L., and R. Neira, Convective growth rate of ion cyclotron waves in a H^+ - He^+ and H^+ - He^+ - O^+ plasma, *J. Geophys. Res.*, *88*, 2170, 1983.

Gonzalez, W. D., B. T. Tsurutani, A. L. C. Gonzalez, E. J. Smith, F. Tang, and S.-I. Akasofu, Solar wind-magnetosphere coupling during intense magnetic storms (1978–1979), *J. Geophys. Res.*, *94*, 8835, 1989.

Gonzalez, W. D., J. A. Joselyn, Y. Kamide, H. W. Kroehl, G. Rostoker, B. T. Tsurutani, and V. M. Vasyliunas, What is a geomagnetic storm?, *J. Geophys. Res.*, *99*, 5771, 1994.

Gorbachev, O. A., G. V. Khazanov, K. V. Gamayunov, and E. N. Krivorutsky, A theoretical model for the ring current interaction with the Earth's plasmasphere, *Planet. Space Sci.*, *40*, 859, 1992.

Gringauz, K. I., Plasmasphere and its interaction with ring current, *Space Sci. Rev.*, *34*, 245, 1983.

Gringauz, K. I., Structure and properties of the Earth plasmasphere, *Adv. Space Res.*, *5*, 391, 1985.

Hinton, F. L., Collisional transport in plasma, in *Handbook of Plasma Physics*, vol. 1, edited by A. A. Galeev and R. N. Sudan, North-Holland, New York, 1983.

Horwitz, J. L., C. R. Baugher, C. R. Chappell, E. G. Shelley, D. T. Young, and R. R. Anderson, ISEE 1 observations of thermal plasma during periods of quieting magnetic activity, *J. Geophys. Res.*, *86*, 9989, 1981.

Johnson, J. R., and C. Z. Cheng, Can ion cyclotron waves propagate to the ground?, *Geophys. Res. Lett.*, *26*, 671, 1999.

Jordanova, V. K., J. U. Kozyra, G. V. Khazanov, A. F. Nagy, C. E. Rasmussen, and M.-C. Fok, A bounce-averaged kinetic model of the ring current ion population, *Geophys. Res. Lett.*, *21*, 2785, 1994.

Jordanova, V. K., L. M. Kistler, J. U. Kozyra, G. V. Khazanov, and A. F. Nagy, Collisional losses of ring current ions, *J. Geophys. Res.*, *101*, 111, 1996a.

Jordanova, V. K., J. U. Kozyra, and A. F. Nagy, Effects of heavy ions on the quasi-linear diffusion coefficients from resonant interactions with EMIC waves, *J. Geophys. Res.*, *101*, 19,771, 1996b.

Jordanova, V. K., J. U. Kozyra, A. F. Nagy, and G. V. Khazanov, Kinetic model of the ring current-atmosphere interactions, *J. Geophys. Res.*, *102*, 14,279, 1997.

Jordanova, V. K., C. J. Farrugia, L. Janoo, J. M. Quinn, R. B. Torbert, K. W. Ogilvie, R. P. Lepping, J. T. Steinberg, D. J. McComas, and R. D. Belian, October 1995 magnetic cloud and accompanying storm activity: Ring current evolution, *J. Geophys. Res.*, *103*, 79, 1998a.

Jordanova, V. K., C. J. Farrugia, J. M. Quinn, R. M. Thorne, K. W. Ogilvie, R. P. Lepping, G. Lu, A. J. Lazarus, M. F. Thomsen, and R. D. Belian, Effect of wave-particle interactions on ring current evolution for January 10–11, 1997: Initial results, *Geophys. Res. Lett.*, *25*, 2971, 1998b.

Jordanova, V. K., C. J. Farrugia, R. M. Thorne, G. V. Khazanov, G. D. Reeves, and M. F. Thomsen, Modeling ring current proton precipitation by EMIC waves during the May 14–16, 1997, storm, *J. Geophys. Res*, *106*, 7, 2001.

Kennel, C. F., and H. E. Petschek, Limit on stably trapped particle fluxes, *J. Geophys. Res.*, *71*, 1, 1966.

Khazanov, G. V., K. V. Gamayunov, V. K. Jordanova, and E. N. Krivorutsky, A self-consistent model of the interacting ring current ions and electromagnetic ion cyclotron waves, initial results: Waves and precipitating fluxes, *J. Geophys. Res.*, *107*(A6), 1085, doi:10.1029/2001JA000180, 2002.

Knudsen, D. J., M. C. Kelley, and J. F. Vickrey, Alfvén waves in the auroral ionosphere: A numerical model compared with measurements, *J. Geophys. Res.*, *97*, 77, 1992.

Kozyra, J. U., T. E. Cravens, A. F. Nagy, E. G. Fontheim, and R. S. B. Ong, Effects of energetic heavy ions on electromagnetic ion cyclotron wave generation in the plasmapause region, *J. Geophys. Res.*, *89*, 2217, 1984.

Kuramitsu, Y., and T. Hada, Acceleration of charged particles by large amplitude MHD waves: Effect of wave spatial correlation, *Geophys. Res. Lett.*, *27*, 629, 2000.

LaBelle, J., R. A. Treumann, W. Baumjohann, G. Haerendel, N. Sckopke, G. Paschmann, and H. Lühr, The duskside plasmapause/ring current interface: Convection and plasma wave observations, *J. Geophys. Res.*, *93*, 2573, 1988.

Lepping, R. P., et al., The Wind magnetic field investigation, *Space Sci. Rev.*, *71*, 207, 1995.

Lessard, M. R., and D. J. Knudsen, Ionospheric reflection of small-scale Alfvén waves, *Geophys. Res. Lett.*, *28*, 3573, 2001.

LeVeque, R. J., *Numerical Methods for Conservation Laws*, 2nd ed., Birkhauser Boston, Cambridge, Mass., 1992.

Lyatsky, W. B., and Yu. P. Maltsev, *The magnetosphere-ionosphere interaction*, Nauka, Moscow, 1983.

Lyons, L. R., Pitch angle and energy diffusion coefficients from resonant interactions with ion-cyclotron and whistler waves, *J. Plasma Phys.*, *12*, 417, 1974.

Lyons, L. R., and D. J. Williams, *Quantitative Aspects of Magnetospheric Physics*, D. Reidel, Norwell, Mass., 1984.

Lysak, R. L., Propagation of Alfvén waves through the ionosphere: Dependence on ionospheric parameters, *J. Geophys. Res.*, *104*, 10,017, 1999.

Mauk, B. H., Helium resonance and dispersion effects on geostationary Alfvén/ion cyclotron waves, *J. Geophys. Res.*, *87*, 9107, 1982.

Maynard, N. C., and A. J. Chen, Isolated cold plasma regions: Observations and their relation to possible production mechanisms, *J. Geophys. Res.*, *80*, 1009, 1975.

Ogilvie, K. W., et al., SWE, A comprehensive plasma instrument for the Wind spacecraft, *Space Sci. Rev.*, *71*, 55, 1995.

Phaneuf, R. A., R. K. Janev, and M. S. Pindzola, Atomic data for fusion, *Collisions of Carbon and Oxygen ions with electrons, H, H_2 and He*, vol. 5, *Tech. Rep. ORNL-6090/V5*, Oak Ridge Natl. Lab., Oak Ridge, Tenn., 1987.

Potter, D., *Computational Physics*, John Wiley, Hoboken, N. J., 1973.

Rairden, R. L., L. A. Frank, and J. D. Craven, Geocoronal imaging with Dynamics Explorer, *J. Geophys. Res.*, *91*, 13,613, 1986.

Rasmussen, C. E., S. M. Guiter, and S. G. Thomas, Two-dimensional model of the plasmasphere: Refilling time constants, *Planet. Space Sci.*, *41*, 35, 1993.

Roux, A., S. Perraut, J. L. Rouch, C. de Villedary, G. Kremser, A. Korth, and D. T. Young, Wave-particle interactions near Ω_{He+} observed on board GEOS 1 and 2: 2. Generation of ion cyclotron waves and heating of He^+ ions, *J. Geophys. Res.*, *87*, 8174, 1982.

Rowland, D. E., and J. R. Wygant, Dependence of the large-scale, inner magnetospheric electric field on geomagnetic activity, *J. Geophys. Res.*, *103*, 14,959, 1998.

Schulz, M., and J. B. Blake, Analytical estimates for gyration-, bounce-, and drift-averaged atmospheric densities experienced by geomagnetically trapped particles, *Eos Trans. AGU*, *71*, 1556, 1990.

Scudder, J., et al., HYDRA—A 3-dimensional electron and ion hot plasma instrument for the Polar spacecraft of GGS mission, *Space Sci. Rev.*, *71*, 459, 1995.

Sheldon, R. B., and D. C. Hamilton, Ion transport and loss in the Earth's quiet ring current: 1. Data and standard model, *J. Geophys. Res.*, *98*, 13,491, 1993.

Smith, P. H., and R. A. Hoffman, Ring current particle distributions during the magnetic storms of 16–18 December 1971, *J. Geophys. Res.*, *78*, 4731, 1973.

Stern, D. P., The motion of a proton in the equatorial magnetosphere, *J. Geophys. Res.*, *80*, 595, 1975.

Stix, T. H., *The Theory of Plasma Waves*, McGraw Hill, New York, 1962.

Tsurutani, B. T., and W. D. Gonzalez, The interplanetary causes of magnetic storms: A review, in *Magnetic Storms*, *Geophys. Monogr. Ser.*, vol. 98, edited by B. T. Tsurutani et al., p. 77, AGU, Washington, D. C., 1997.

Volland, H., A semiempirical model of large-scale magnetospheric electric fields, *J. Geophys. Res.*, *78*, 171, 1973.

Wentworth, R. C., Enhancement of hydromagnetic emissions after geomagnetic storms, *J. Geophys. Res.*, *69*, 2291, 1964.

Williams, D. J., Ring current composition and sources, in *Dynamic of Magnetosphere*, edited by S.-I. Akasofu, p. 407, D. Reidel, Norwell, Mass., 1980.

Williams, D. J., Ring current composition and sources: An update, *Planet. Space Sci.*, *29*, 1195, 1981.

Yanenko, N. N., *The Method of Fractional Steps: The Solution of Problems of Mathematical Physics in Several Variables*, Springer-Verlag, New York, 1971.

Young, D. T., T. J. Geiss, H. Balsiger, P. Eberhardt, A. Ghiedmetti, and H. Rosenbauer, Discovery of He^{2+} and O^{2+} ions of terrestrial origin in the outer magnetosphere, *Geophys. Res. Lett.*, *4*, 561, 1977.

Young, D. T., S. Perraut, A. Roux, C. de Villedary, R. Gendrin, A. Korth, G. Kremser, and D. Jones, Wave-particle interactions near Ω_{He+} observed on GEOS 1 and 2: 1. Propagations of ion cyclotron waves in He^+-rich plasma, *J. Geophys. Res.*, *86*, 6755, 1981.

Young, D. T., H. Balsiger, and J. Geiss, Correlations of magnetospheric ion composition with geomagnetic and solar activity, *J. Geophys. Res.*, *87*, 9077, 1982.

K. V. Gamayunov, Geophysical Institute, University of Alaska Fairbanks, 903 Koyukuk Drive, P. O. Box 757320, Fairbanks, AK 99775, USA. (gamayunov@gi.alaska.edu)

V. K. Jordanova, Space Science Center, University of New Hampshire, Durham, NH 03824, USA. (vania.jordanova@unh.edu)

G. V. Khazanov, Space Science Department, National Space Science and Technology Center, NASA Marshall Space Flight Center, 320 Sparkman Drive, Huntsville, AL 35805, USA. (george.khazanov@msfc.nasa.gov)